EARTH SURFACE PROCESSES AND LANDFORMS
*Earth Surf. Process. Landforms* **38**, 1623–1641 (2013)

Published online 8 May 2013 in Wiley Online Library
(wileyonlinelibrary.com) DOI: 10.1002/esp.3395

# Sediment routing hypothesis for pool-riffle maintenance

**David J. Milan***
Department of Geography, Environment and Earth Sciences, University of Hull, Hull, UK

Received 17 August 2012; Revised 21 January 2013; Accepted 22 January 2013

*Correspondence to: David J. Milan, Department of Geography, Environment and Earth Sciences, University of Hull, Hull, HU6 7RX, UK. E-mail: d.milan@hull.ac.uk

ESPL
Earth Surface Processes and Landforms

ABSTRACT: This paper provides comprehensive evidence that sediment routing around pools is a key mechanism for pool-riffle maintenance in sinuous upland gravel-bed streams. The findings suggest that pools do not require a reversal in energy for them to scour out any accumulated sediments, if little or no sediments are fed into them. A combination of clast tracing using passive integrated transponder (PIT) tagging and bedload traps (positioned along the thalweg on the upstream riffle, pool entrance, pool exit and downstream riffle) are used to provide information on clast pathways and sediment sorting through a single pool-riffle unit. Computational fluid dynamics (CFD) is also used to explore hydraulic variability and flow pathways. Clast tracing results provide a strong indication that clasts are not fed through pools, rather they are transported across point bar surfaces, or around bar edges (depending upon previous clast position, clast size, and event magnitude). Spatial variations in bedload transport were found throughout the pool-riffle unit. The pool entrance bedload trap was often found to be empty, when the others had filled, further supporting the notion that little or no sediment was fed into the pool. The pool exit slope trap would occasionally fill with sediment, thought to be sourced from the eroding outer bank. CFD results demonstrate higher pool shear stresses ($\tau \approx 140$ N m$^{-2}$) in a localized zone adjacent to an eroding outer bank, compared to the upstream and downstream riffles ($\tau \approx 60$ N m$^{-2}$) at flows of $6 \cdot 2$ m$^3$ s$^{-1}$ ($\approx 60\%$ of the bankfull discharge) and above. There was marginal evidence for near-bed velocity reversal. Near-bed streamlines, produced from velocity vectors indicate that flow paths are diverted over the bar top rather than being fed through the thalweg. Some streamlines appear to brush the outer edge of the pool for the $4 \cdot 9$ m$^3$ s$^{-1}$ to $7 \cdot 8$ m$^3$ s$^{-1}$ (between 50 and 80% of the bankfull discharge) simulations, however complete avoidance was found for discharges greater than this. Copyright © 2013 John Wiley & Sons, Ltd.

KEYWORDS: pool-riffle maintenance; velocity reversal; clast tracing; CFD; sediment transport; gravel-bed river

## Introduction

Pools and riffles are mesoscale bedforms found in moderate slope river channels (< 5%; e.g. Montgomery *et al.*, 1995). The bedforms are important for creating a variety of ecological niches for various in-stream species, as a result of spatial and temporal hydraulic variability, and associated bed grain size character. Research into the mechanisms for pool-riffle maintenance have current significance for environmentally sensitive river engineering and rehabilitation (Emery *et al.*, 2003; Sear and Newson, 2004; Wheaton *et al.*, 2004a; Pasternack *et al.*, 2008; Biron *et al.*, 2011). The remodelling of river reaches incorporating pools, riffles, bars and meanders as well as the introduction of 'designed' substrates to provide spawning habitat for fish is increasingly being applied to degraded reaches of river, for example those degraded through flow regulation (Wheaton *et al.*, 2004b) or channelization. The morphological design of rehabilitated reaches and the prescription of appropriate grain sizes, increasingly uses geomorphological and fisheries data as a template on which to base the rehabilitation project. River rehabilitation projects that re-introduce pool-riffle bedforms must take into consideration the maintenance of the bedform, in order for the project to be sustainable. However, over 40 years on from the first proposed model of maintenance (Keller, 1971), the mechanisms responsible for pool-riffle maintenance are the subject of continued research and debate (Thompson, 2011).

### Pool-riffle maintenance

In simple terms, pool-riffle maintenance refers to the processes by which the pools (low points on the bed long profile) are prevented from being filled from sediment fed and delivered from upstream, and the riffles (high points along the bed long profile) are prevented from being scoured away. For the majority of the flow range the tractive force in the pool is lower in comparison to the adjacent riffles. Any sediment capable of being transported on the riffles is therefore likely to be deposited in the pools, thus filling the pool and lowering the elevation of the riffle. Keller (1971) proposed the velocity reversal hypothesis for pool-riffle maintenance. His data from Dry Creek, California, USA, demonstrated that pool velocities increased at a faster rate in comparison to the riffles for a given incremental rise in discharge. Although he was not able to measure a reversal in velocity, he was able to measure a velocity convergence (equal tractive force), and he hypothesized that the pool velocity would exceed the riffle velocity at bankfull discharge. Keller and Florsheim (1993) were later able to simulate reversal for the same

reach using a one-dimensional (1D) hydraulic model. Using Kellers original data, MacWilliams *et al.* (2006) have also used computational fluid dynamics (CFD) to simulate reversal at the Dry Creek site. This hypothesis provided a mechanism for any accumulated sediment in the pools to be flushed out onto the downstream riffle, whereby riffles acted as high flow storage zones and pools as zones of scour. In this manner the pool-riffle morphology could be maintained.

A number of studies have linked sediment transport processes to Keller's hydraulic model of maintenance, and are conceptualized in Figure 1. Jackson and Beschta's (1982) two-phase sediment transport model suggests that below the reversal threshold and for most of the flow range (Figure 1a), Phase 1 transport (sand) dominates. At these flows the riffle armour remains intact, however sand may be transported into the pool over the stable (armoured) gravel bed provided there is enough supply. Lisle (1979) and Lisle and Hilton (1992) have demonstrated that pools are important storage zones for sand, and have demonstrated the importance of flow stage and sand supply upon sand volumes found in pools. Pool beds composed of coarse lag gravels would be visible at low flow if fine sediment is supply limited, however fines may cover coarse lag in high supply scenarios.

At between 30 and 70% bankfull discharge, gravel transport (Phase 2) is initiated as the surface armour is disrupted on the riffles and coarse bedload is transported downstream. If the tractive force of the riffles is still greater than that of the pools, then pools may begin to fill with gravel at this stage (Clifford and Richards, 1992) (Figure 1b). Some pool scour and exit slope deposition may also occur. As pool tractive force rises further it may eventually exceed that of the adjacent riffles. During this condition (e.g. 70–90% bankfull, Figure 1c), any accumulated pool sediment will scour, and any gravel that is fed into the pool from an upstream riffle will be transported through the pool to the downstream riffle. At bankfull discharge (Figure 1d) pool tractive force exceeds that of the adjacent riffles and transports sediment at a faster rate than the riffles. The outer bank of the pool erodes and deposition occurs on point bars and riffles. It is these sediment transport processes which are thought to be responsible for the observed variations in sorting of the surface layer of sediments between pools and riffles, with riffles most commonly reported as being coarser and better sorted than pools (Table I). Differences in surface grain-size between pools and riffles also influence bed roughness and thus channel hydraulics. One-dimensional hydraulic modelling reported by Carling and Wood (1994) has shown that pools that are hydraulically rougher are more likely to show tractive force reversal.

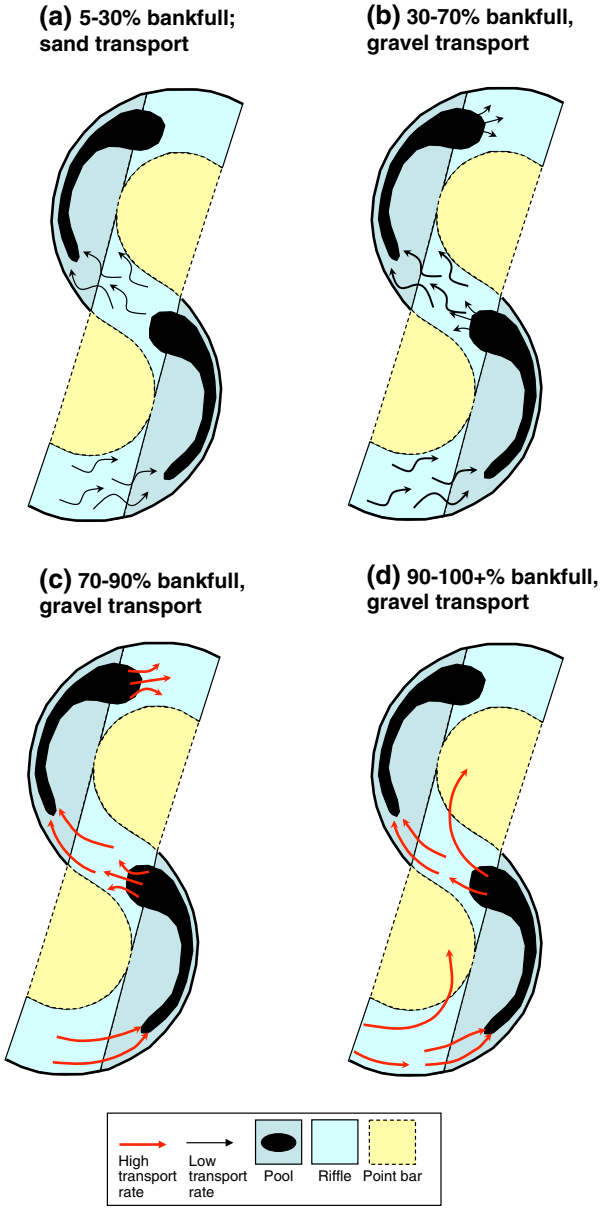


**Figure 1.** Conventional sediment routing model, incorporating hydraulic reversal. The model demonstrates processes occurring at different flow stages as a proportion of the bankfull discharge, tentatively based upon Lisle (1979), Jackson and Beschta (1982), and Lisle and Hilton (1992). This figure is available in colour online at wileyonlinelibrary.com/journal/espl

## Reversal hypothesis issues

Despite the elegance of Keller's hypothesis, a number of workers have disputed velocity reversal, largely due to the principle of mass continuity. Velocity reversal (cross-section average) requires the wetted cross-section of the pool to be narrower compared to that of the adjacent riffles. However a number of workers (e.g. Richards, 1978; Carling, 1991; Carling and Wood, 1994; Thompson *et al.*, 1999) have demonstrated larger cross-sections for the pool, suggesting that cross-section averaged velocity reversal is not possible. A number of studies have shown reversal occurrence (e.g. Andrews, 1979; Lisle, 1979; Teisseyre, 1984; Ashworth, 1987; Petit, 1987; Sear, 1996; Milan *et al.*, 2001), some have found that with increasing discharge the velocity increases at a faster rate through the pool than over the riffle, but have not observed reversal (Keller, 1971; Richards, 1976a, 1976b, 1978; Jackson and Beschta, 1982; Carling, 1991; Clifford and Richards, 1992; Carling and Wood, 1994; Robert, 1997), whilst some studies oppose velocity reversal (Teleki, 1972; Bhowmik and Demissie, 1982). This debate has prompted further studies into pool-riffle maintenance processes, and a number of alternative hypothesis have since been proposed which do not require tractive force reversal including (a) the role of bed sediment structure leading to differential bed mobility between the pool and riffle (Clifford, 1993; Sear, 1996; Hodge *et al.*, 2012), (b) sediment continuity whereby scour and pool maintenance occurs in parts of the channel with a positive downstream shear stress gradient, and deposition and riffle maintenance occurs in parts of the channel with a negative downstream shear stress gradient (Wilkinson *et al.*, 2004), (c) the role of obstructions in the pool e.g. boulders in 'forced pools' or log jams and tree roots in alluvial pool-riffle channels causing (i) a reduction in channel cross-section area and (ii) influencing turbulent flow structures, thought to be responsible for localized scour (Thompson *et al.*, 1996, 1999; Buffington *et al.*, 2002; MacWilliams *et al.*, 2006; Harrison and Keller, 2007; MacVicar and Roy, 2007a, 2007b; Thompson, 2007).

**Table I.** Summary of a range of studies documenting textural differences between the bed sediments of riffles and pools

| Investigator | River | Riffle | Pool |
|---|---|---|---|
| Hack (1957) | Zekiah Swamp basin, and Mataponi Creek, USA | No difference | No difference |
| Leopold *et al.* (1964) | Seneca Creek, Maryland, USA | $D_{50} = 17$ mm | $D_{50} = 6$ mm |
| Yang (1971) | Lab flume and Kaskaskia River, Illinois, USA | Coarser | Finer |
| Keller (1971, 1972) | Dry Creek, USA | $D_{50} = 32$ mm | $D_{50} = 10$ mm |
| Church (1972) | Baffin Island rivers, Canada | Coarser | Finer |
| Cherkauer (1973) | Treia River, Italy | Cobbles and boulders, little matrix | Sand and fine gravel |
| Richards (1976a, 1976b, 1978) | River Fowey, Cornwall, UK | 45–60 mm | 37–52 mm |
| Lisle (1979), Andrews (1983) | East Fork River, Wyoming, USA | Coarser at low flow, finer at high flow | Finer at low flow, coarser at high flow |
| Milne (1982) | Kingledoors Burn, Tweed, Scotland, UK | $D_{50} = 43$ mm | $D_{50} = 36$ mm |
| Bhowmik and Demissie (1982) | Kaskaskia River, Illinois, USA | Coarser<br>$D_{max} = 46$ mm | Finer<br>$D_{min} = 0 \cdot 034$ mm |
| Hirsch and Abrahams (1984) | Cattaraugus Creek, New York, USA | Coarser and better sorted, $D_x = 57$ mm | Finer and less well sorted, $x = 28$ mm |
| Ashworth (1987) | Allt Dubaig, Scotland, | $D_{50} = 113$ mm | $D_{50} = 125$ mm |
| | Reach A | $D_{50} = 87$ mm | $D_{50} = 120$ mm |
| | Reach B | $D_{50} = 70$ mm | $D_{50} = 59$ mm |
| | Reach C | $D_{50} = 78$ mm | $D_{50} = 64$ mm |
| | Reach D | $D_{50} = 40$ mm | $D_{50} = 40$ mm |
| | Reach E | $D_{50} = 62$ mm | $D_{50} = 70$ mm |
| | River Feshie, Scotland, UK | | |
| Petit (1987) | La Rulles, Ardenne, France | $15 \cdot 2$ mm | 50–100 mm |
| Carling (1991) | River Severn, Shrewsbury, UK | $D_{50} = 25$ mm | $D_{50} = 43$ mm |
| Clifford (1993) | River Quarme, Exmoor, UK | Coarser | Finer |
| Sear (1996) | River North Tyne, UK | $D_{50} = 60$ mm | $D_{50} = 43$ mm |
| Robert (1997) | Little Rouge River, Ontario, Canada | Coarser | Finer |
| Thompson *et al.* (1996, 1999) | North Saint Vrain Creek, Colorado, USA | Finer<br>Mean difference = $4 \cdot 8$ mm<br>Max difference = $8 \cdot 8$ mm<br>Reach $D_{50} = 95$ mm | Coarser |
| Wilkinson *et al.* (2000) | Steavenson River, Marysville, Victoria, Australia | 76 mm | 50 mm |
| Wilkinson *et al.* (2008) | Morses Creek, Wandiligong, Victoria, Australia | 130 mm | 50 mm |
| Caamaño et al. (2010) | Red river, North Central Idaho, USA | 56 mm | 44 mm |

Wilkinson *et al*. (2008) highlight that a better understanding of pool-riffle maintenance may be gained through further research into bar instability processes. Surprisingly, to date these two research streams have seen little cross-fertilization. Dietrich *et al*. (1979) and Dietrich and Smith (1984) however provide a detailed account of sediment transport for a meander bend with a point bar on Muddy Creek, Wyoming. Instead of coarse bedload following the thalweg, as is assumed in the pool-riffle literature, these workers found that the maximum zone of bedoad transport followed an outward-shifting zone of maximum shear stress; where at high flow bedload was concentrated on the inner bank as it enters the meander and was then fed outward across the bar surface towards the pool. Clasts would then fall down the avalanche face of the bar into the pool, against the direction of weak inward secondary circulation. Conversely fine suspended sediment would initially follow the thalweg around the meander bend, but get deflected by secondary flow currents. Coarse and fine fractions were found to cross paths on the top of the point bar. Although pool-riffle maintenance was not discussed by Dietrich and Smith (1984), it is likely that pool maintenance would have required hydraulic reversal to remove the coarse bedload being fed into it from across the bar surface. Keller and Florsheim (1993) highlight that hydraulics and sediment transport processes are more complex in meandering than in straight channels, and that processes that keep the bed material out of the pool centre or that promote scour in the pool should be considered further.

Although Milan *et al*. (2001) demonstrated marginal section-averaged velocity reversal for four out of six pool-riffle units for the River Rede, UK, clast tracing work on the same reach of river (Milan, 2000; Milan *et al*., 2002) also suggested that clast routing and the role of point-bars were important for the maintenance of the bedform. These workers found that gravel appeared not to be fed into pools, rather clasts were routed from upstream riffle to bar, and then to the downstream riffle. CFD work conducted by Booker *et al*. (2001) further supports the notion that sediment may not be fed into pools, as their simulations demonstrate near bed flow routing away from pool troughs. If sediments are not fed into pools, then tractive force reversal may not be required to maintain the bedform hence offering a possible new and alternative hypothesis for pool-riffle maintenance. This investigation uses a combination of sediment tracing, trapping and CFD, to further explore this alternative hypothesis of pool-riffle maintenance and aims to (a) investigate the role of sediment routing in the maintenance of pools and riffles and (b) investigate spatial patterns of sediment transport and sorting through a pool-riffle sequence.

## Study Location

The study was conducted on a 250 m reach of the River Rede, a headwater tributary to the river North Tyne in Northumberland, UK (Figure 2). Here the Rede has a Strahler stream order of four and is a single-thread, sinuous gravel-bed channel with well developed pool-riffle morphology. The Rede drains a catchment of 18 $km^2$ upstream of the site, with an impermeable geology of Carboniferous sandstones and shales overlain by peat and till. The mean annual runoff is 1026 mm and the flow regime is flashy. Bankfull discharge recorded at the study reach, and supported by post-flood trash line observations, is approximately 10 $m^3\ s^{-1}$. Overall, the bed surface for riffle sediments was finer ($D_{16}$ = 46 mm; $D_{50}$ = 83 mm; $D_{84}$ = 146 mm) than the pools ($D_{16}$ =71 mm; $D_{50}$ = 109 mm; $D_{84}$ = 167 mm). Furthermore, the grain-size of the point bar surfaces was finer than the riffles ($D_{16}$ =26 mm; $D_{50}$ = 52 mm; $D_{84}$ = 95 mm). Bankfull channel width is between 9 and 18 m and the average bankfull channel depth is 0 · 7 m. The mean gradient of the bed throughout the reach is 0 · 006. Results presented in this paper focus upon a single 110 m length pool-riffle unit towards the head of the reach (Figures 2b and 2c).

## Methodology

This study uses sediment tracing and trapping to provide information on sediment transport pathways and sorting. Tracer pathway data are presented following a series of eight flood events. Tracers were emplaced on 5 November 2006, and re-surveyed on eight occasions following flood events (Table II). Data are also presented from continuous recording bedload traps positioned throughout a single pool-riffle unit. Although these were installed in the study reach during October 2004, they were not fully operational until 1 November 2005. Summary grain size data are presented for the contents of sediment traps emptied on eight different occasions following sediment transport (25/11/05; 13/12/05; 5/1/06; 7/2/06; 7/6/06; 4/11/06; 15/1/07; 3/3/07). Fifteen-minute interval load cell data from the traps are presented for a series of five flood events that occurred between 7 and 15 January 2007, to demonstrate spatial variations in sediment transport rate, and between-trap differences in the timing of the onset of sediment transport. CFD is used to provide information on tractive force and near bed flow trajectories.

### Clast tracing

Passive integrated transponder (PIT) tags were inserted into 98 clasts ($D_{16}$ = 54 mm, $D_{50}$ = 78 mm, $D_{84}$ = 110 mm) selected at random from the bed surface at the study site (Figure 2c). The $D_{min}$ was 33 mm, limited by the ability to insert the 20 mm long PIT, and the $D_{max}$ was 197 mm. The grain size of the tracers was slightly finer than that recorded for the reach as a whole. PIT tags have been used in a number of recent studies investigating sediment transport dynamics (e.g. Lamarre *et al*., 2005; Lamarre and Roy, 2008; MacVicar and Roy, 2010; Biron *et al*., 2011). Lamarre *et al*. (2005) provides further details on the hardware employed. Each PIT can be programmed with a unique identification, and can be detected, using a search loop antenna system linked to a laptop, even when the clast is buried by up to 0 · 5 m. Importantly for sediment transport investigations, this permits clasts to be tracked without them being disturbed. Detection of two tracers positioned close to each other did not appear to cause a problem as both PIT codes could be detected. However, close positioning of multiple tracers could potentially introduce detection issues. Tracers were seeded throughout the pool-bar-riffle unit, by placing 10 clasts across 10 cross-sections, each approximately 10 m apart (Figure 3a). Each clast was then surveyed using a Leica 500 differential global positioning system (dGPS), to a vertical accuracy of 10 mm + 1 ppm and a horizontal accuracy of 20 mm + 2 ppm. Re-surveys of the tracer clasts, following search loop detection and dGPS survey, were undertaken on eight occasions following introduction of the clasts to the river, between 5 November 2006 and 11 May 2008 following a range of geomorphically effective flows, including two overbank events (Table II).

### Bedload traps

Four continuous recording bedload traps based upon the design of Sear *et al*. (2000) were installed at the study site in October 2004. In order to detect spatial patterns in bedload transport through the pool-riffle unit, traps were positioned

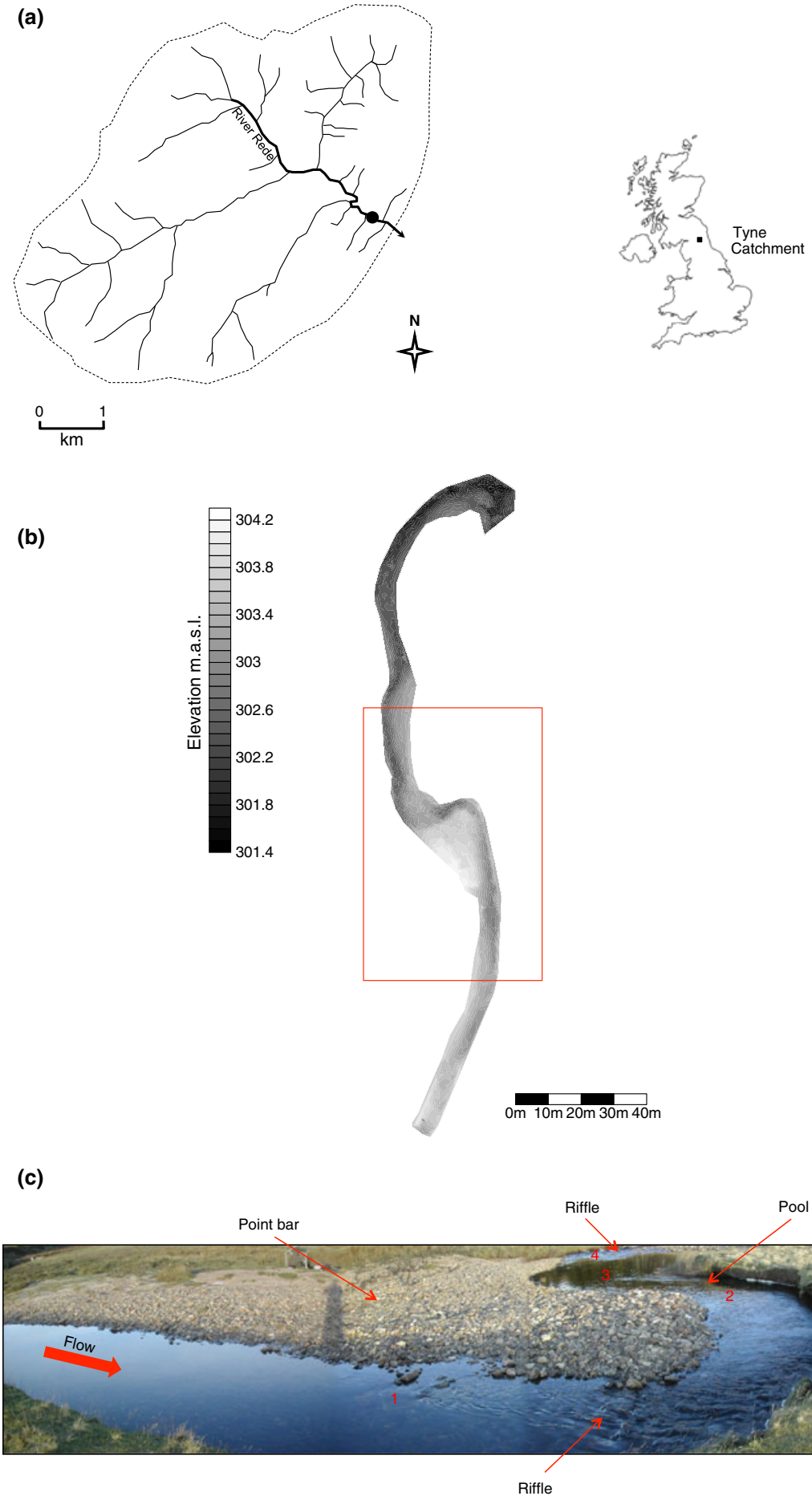


**Figure 2.** Study site location (a) catchment map, (b) shaded relief map of full study reach used for flow simulations. Results presented in this paper focus upon the single pool-riffle unit highlighted by the red box, (c) photograph of pool riffle unit showing the locations of sediment traps 1–4. This figure is available in colour online at wileyonlinelibrary.com/journal/espl

**Table II.** Event sequence, and magnitude

| | Duration between tracer re-surveys | Discharge ($m^3$ $s^{-1}$) |
|---|---|---|
| Event 1 | 05/11/06–18/12/06 | 7·8 (± 0·39) |
| Event 2 | 18/12/06–15/01/07 | 11·5 (± 0·58) |
| Event 3 | 15/01/07–04/03/07 | 4·9 (± 0·23) |
| Event 4 | 04/03/07–02/04/07 | 9·0 (± 0·45) |
| Event 5 | 02/04/07–16/08/07 | 8·1 (± 0·40) |
| Event 6 | 16/08/07–10/11/07 | 5·0 (± 0·24) |
| Event 7 | 10/11/07–16/12/08 | 11·9 (± 0·60) |
| Event 8 | 16/12/08–11/05/08 | 6·2 (± 0·31) |

Stage was measured using a Sentry pressure transducer located at the upstream end of the study reach, and discharges predicted from the stage-discharge rating relation. Error is indicated in brackets.

along the thalweg on an upstream riffle, pool entrance, pool exit slope and downstream riffle (Figures 2c and 3a). The traps, built from 5 mm sheet aluminium, comprise an inner (0·545 m × 0·400 m × 0·315 m) and an outer box (0·610 m × 0·465 m × 0·450 m) with a hinged lid, and an aperture (0·220 × 0·330 m) to allow bedload entry. This aperture was about 11% of the low flow wetted channel width at the pool entrance, and only about 2% of the bankfull wetted width (including the point bar surface). It was therefore possible that sediment transport could take place in the vicinity of the trap without being detected, if the sediment missed the aperture. The inner box has a capacity of 0·066 $m^3$ and sits on a specially designed cradle that distributes mass evenly over a load cell. The load cell is connected by buried cable to a bankside data logger that recorded a calibrated mass every 15 minutes (between 7 and 15 January 2007). In phase with the bedload trap measurements, stage was recorded every 15 minutes. Sediment samples were retrieved from the traps following flood events on eight occasions (between 1 November 2005 and 3 March 2007). Grain-size data for each trap were obtained after dry sieving the sediment samples.

## CFD modelling

The CFD code used in this investigation was version 1.1 of SSIIM (Sediment Simulation in Intakes with Multiblock option; Olsen, 2004). The model has been applied previously to model free surface flow dynamics of gravel-bed rivers in the UK, in particular to address hydraulics and sediment transport processes through pool-riffle sequences (Booker *et al.*, 2001; Clifford *et al.*, 2005; Clifford *et al.*, 2010) and hydraulic modelling of fish habitat (Booker, 2003). The model solves the full three-dimensional (3D) Navier–Stokes equations with a $\kappa$-$\varepsilon$ turbulence closer model on a 3D non-orthogonal grid

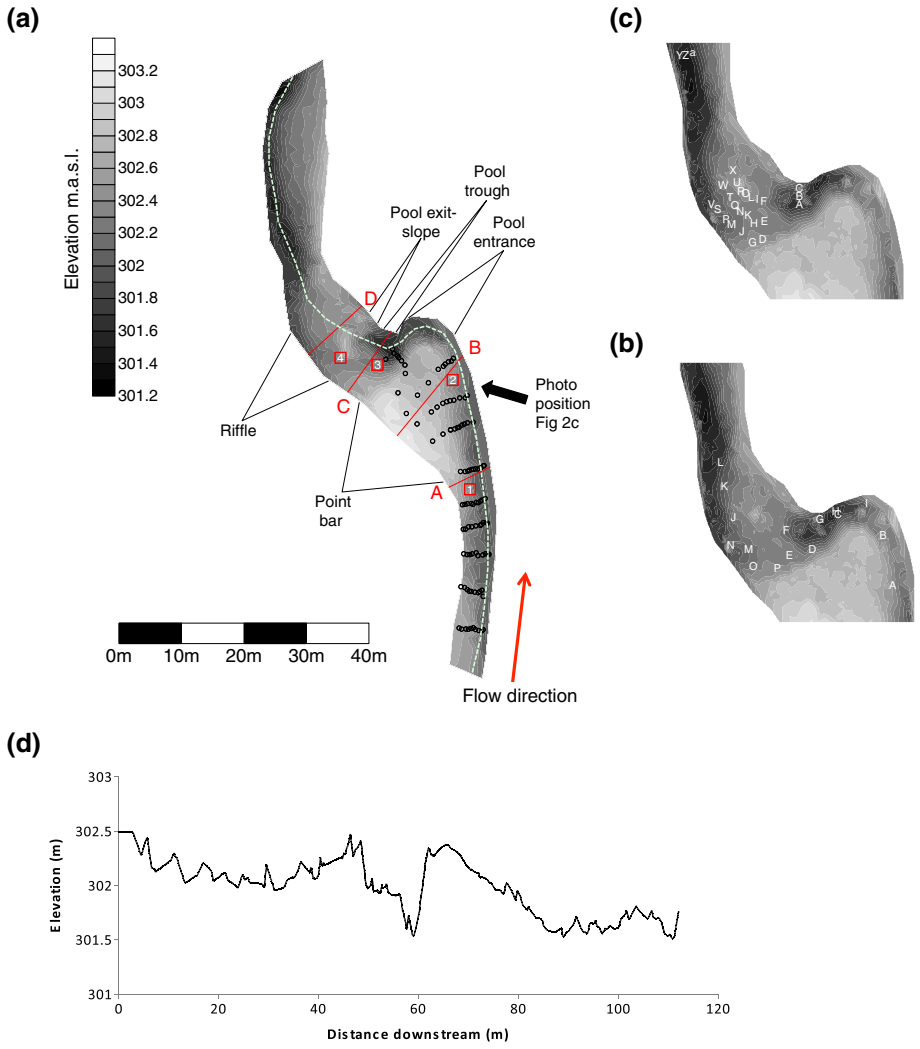


**Figure 3.** (a) Shaded relief map of pool-riffle unit indicating the seeding position of tracer clasts, bedload trap position (numbered 1-4), line taken for long profile (stippled) shown in Figure 3d, and cross-sections demonstrated later in Figure 10, (b) location of velocity and depth measurements for the 1·52 $m^3$ $s^{-1}$ flow validation, (c) location of velocity measurements for the 3·6 $m^3$ $s^{-1}$ flow validation, (d) long profile of pool-riffle unit. This figure is available in colour online at wileyonlinelibrary.com/journal/espl

$$\frac{\partial U_i}{\partial t} + U_j \frac{\partial U_i}{\partial x_j} = \frac{1}{\rho}\frac{\partial}{\partial x_j}\left(-P\delta_{ij} - \overline{\rho u_i u_j}\right) \quad (1)$$

where the term on the left of Equation 1 is the transient term and the next term is the convective term. The first term on the right of Equation 1 is the pressure term, and the second term on the right is the Reynolds stress term. Non-compressible, constant density flow is assumed. The $k$-$\varepsilon$ model is used to calculate turbulent shear stress for the 3D simulations within SSIIM. The eddy-viscosity concept $\upsilon_T$ with the $k$-$\varepsilon$ turbulence closer model is used to model the Reynolds stress term

$$-\overline{u_i u_j} = \nu_T\left(\frac{\partial U_j}{\partial x_i} + \frac{\partial U_i}{\partial x_j}\right) + \frac{2}{3}k\delta_{ij} \quad (2)$$

In Equation 2, the first term on the right side of the equation forms the diffusive term in the Navier–Stokes equation, the second term is often neglected and the third term is incorporated into the pressure. The $k$-$\varepsilon$ model calculates the eddy-viscosity as

$$\upsilon_T = c_\mu \frac{k^2}{\varepsilon} \quad (3)$$

where $k$ is the turbulent kinetic energy, $\varepsilon$ is its dissipation and $c_\mu$ is a constant. Further details of the modelling of $k$ and $\varepsilon$ are given in Olsen (2007). In this study the model was run with a free water surface, for steady-state solutions. The water surface was calculated using the SIMPLE method (Patanker, 1980) for pressure correction. This was used to couple all cells except those closest to the surface and allowed calculation of a free water surface. The water surface is fixed at the downstream cross-section where the pressure, $P_{\text{ref}}$, is taken as a reference. A pressure deficit at each cell is then calculated by subtracting this reference pressure from the extrapolated pressure $P_{ij}$ for each cell and used to move the water surface (Olsen and Kjellesvig, 1998)

$$\Delta h_{ij} = \frac{l}{\rho g}\left(P_{ij} - P_{\text{ref}}\right) \quad (4)$$

Where $l$ is the difference in the height between the water surface at the given and reference points.

Roughness is specified for each boundary cell within the computational mesh according to the law of the wall

$$\frac{U}{u_*} = \frac{1}{\kappa}\ln\left(\frac{30z}{k_s}\right) \quad (5)$$

where $U$ is the average velocity, $u_*$ is the shear velocity, $\kappa$ is the von Karmen constant equal to $0 \cdot 4$, and $k_s$ is the bed roughness, and $z$ is the distance to the wall.

In Equation 5, $k_s$ is theoretically equivalent to the diameter of particles on the bed, but, in practice, $k_s$ is obtained from $n$ using a modification of Strickler's Equation 6 by assuming $k_s$ equates to the $D_{50}$ of the bed sediments

$$n = 0.0151 k_s^{1/6} \quad (6)$$

A value of $n$ is required to fix an initial water surface profile to start the simulation. An initial water surface is calculated for successive upstream locations from the known downstream water surface elevation and a 1D backwater model. Thus, $n$ was adjusted to yield the greatest convergence with known water elevations and the discharge constraint. After this initial calibration, the 3D model surface was allowed to adjust. For the simulations presented in this paper, $n$ was fixed at an optimum value of $0 \cdot 032$ that yielded a skin friction of 90 mm, which is almost equal to the reach $D_{50}$ (87 mm). This similarity in measured (from Wolman grid measurements) and calculated results for skin friction is an encouraging indicator of model suitability.

Boundary shear stress was estimated from

$$\tau = 0.3\rho k \quad (7)$$

following Booker *et al.* (2001).

## Boundary conditions

SSIIM requires the following input variables: (i) the 3D coordinates of the bed; (ii) information on the boundary roughness; (iii) discharge; (iv) water level at the exit cross-section; (v) 3D inlet velocities. The river bed topography of the Rede was surveyed at the start on the investigation using a Leica 500 dGPS. Boundary roughness was also quantified at the outset of the investigation through measurement of the intermediate axis of 100 clasts (Wolman, 1954) taken from pools, riffles, runs and bars for the full study reach used in the flow simulation (Figure 4a). Roughness height was input into the model based on $3 \cdot 5D_{84}$, following Clifford *et al.* (1992). SSIIM also requires the specification of a Strickler value, the derivation of which was described earlier in Equation 6. Bank roughness also needs to be specified, and was ascertained through a calibration process described later. Discharge was measured at a gauging station situated at the upstream end of the study reach. A water surface elevation rating curve was also available for the exit cross-section of the model domain, through the use of a stage board that was surveyed into the same coordinate system as the bed. Measured inflow velocity profiles were not available for the simulations presented here, instead an imposed uniform cross-stream velocity pattern with a vertical logarithmic profile, with zero cross-stream and vertical velocities was applied.

The computational mesh used in the study comprised a total of 120 000 cells; 400 in the stream-wise, 20 in the cross-stream, and 15 in the vertical (e.g. Figure 4b). SSIIM 1 does not simulate wetting and drying. For the lower flow validation simulations ($1 \cdot 5$ m$^3$ s$^{-1}$ and $3 \cdot 6$ m$^3$ s$^{-1}$), blocks were used to simulate bars and dry parts of the channel, knowing the position of the waters edge. Banks were near-vertical in some areas of the model domain, for example around the outer edge of the meander and pool, hence vertical walls were used in the model. The channel topography was interpolated for all the basal grid points of the computational mesh using a linear interpolation scheme.

## Grid dependence

Lane *et al.* (2005) advise that solutions for a range of grid resolutions should be presented to demonstrate grid independence or grid-convergent results. The possible role of secondary flow upon flow vector direction and its influence upon clast transport pathways, were of particular interest in this investigation. The vertical number of grid cells is very important when modelling secondary flows, where at least four cells are required in the vertical to resolve a circulation (Booker, 2003). Grid resolution is also important when modelling near-bed hydraulics, as this zone tends to have the greatest velocity and turbulent kinetic energy gradients. To examine the role of grid dependence further, a similar approach to Booker (2003) was adopted, whereby the $1 \cdot 52$ m$^3$ s$^{-1}$ model was run with three different grid resolutions in the vertical, with all cells distributed evenly throughout the water column (10, 15 and 20 cells). All other boundary conditions were held constant including the number of cells in the $x$-$y$ plane. Velocity profiles for points (A–P), the location of which is shown in Figure 3b, were constructed in order to calculate velocity at $0 \cdot 02$, $0 \cdot 03$, $0 \cdot 04$ and $0 \cdot 05$ m from the bed. Linear regressions were then performed on velocity values for each of these depths, for each combination of grid resolutions. All the comparisons involving runs with 10 cells in the vertical

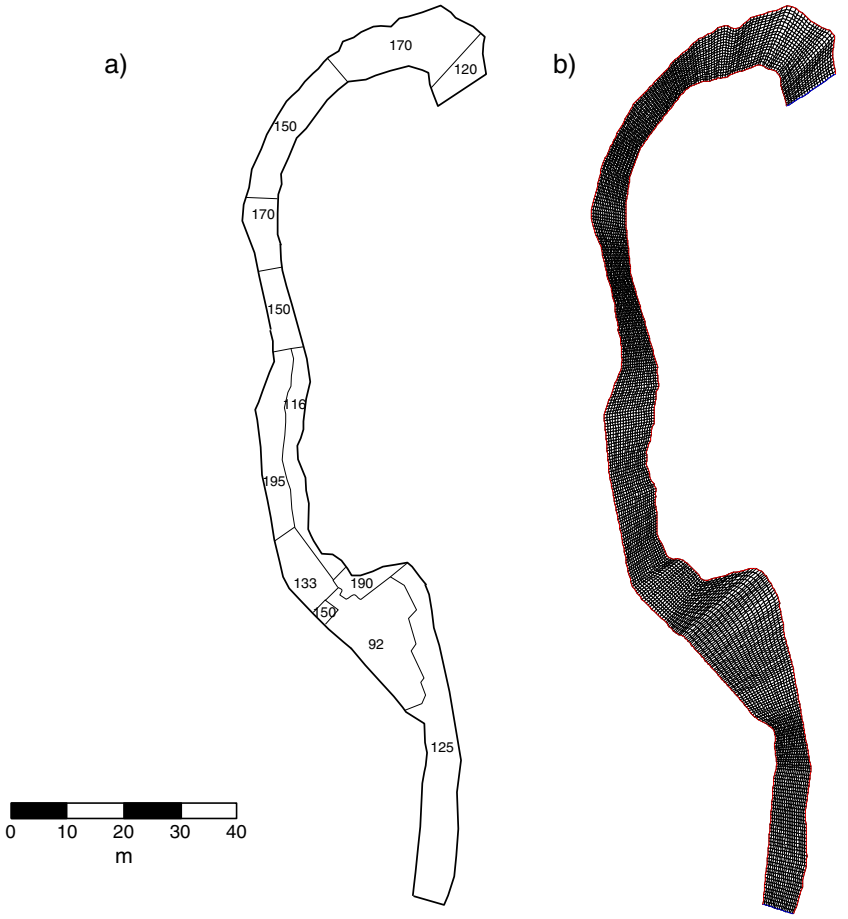


**Figure 4.** (a) Map of bed surface $D_{84}$ (mm) and (b) planview of computational mesh. This figure is available in colour online at wileyonlinelibrary.com/journal/espl

**Table III.** Test of grid dependence through linear regression of simulated velocities at the same height above the bed for different vertical grid resolutions

| Height above bed (m) | Number of cells in $z$ | $m$ | $c$ | $r^2$ |
|---|---|---|---|---|
| 0·02 | 15 × 10 | 0·570 | 0·079 | 0·795 |
| | 20 × 10 | 0·480 | 0·100 | 0·804 |
| | 20 × 15 | 0·817 | 0·040 | 0·951 |
| 0·03 | 15 × 10 | 0·488 | 0·125 | 0·834 |
| | 20 × 10 | 0·487 | 0·147 | 0·731 |
| | 20 × 15 | 1·040 | 0·008 | 0·954 |
| 0·04 | 15 × 10 | 0·483 | 0·155 | 0·841 |
| | 20 × 10 | 0·467 | 0·181 | 0·737 |
| | 20 × 15 | 1·014 | 0·013 | 0·960 |
| 0·05 | 15 × 10 | 0·472 | 0·181 | 0·852 |
| | 20 × 10 | 0·405 | 0·289 | 0·418 |
| | 20 × 15 | 0·870 | 0·127 | 0·507 |

were found to be grid dependent; where the slope exponent ($m$) consistently showed a substantial deviation from one (Table III). Runs that employed vertical grid resolutions of 15 and 20 cells in the vertical were all found to be grid independent, hence this study therefore used 15 cells in the vertical.

## Bank roughness calibration

In the Rede study reach the key roughness elements were gravels; there was no vegetation growing on the banks. Bank roughness was attained through a calibration process, whereby the model was run at the 1·52 $m^3$ $s^{-1}$ discharge with four different bank roughness values ranging from 0·1 m to 0·75 m. This discharge was used to calibrate the wall roughness in preference to the 3·6 $m^3$ $s^{-1}$ flow as it was possible to obtain good spatial distribution of velocity measurements around the bend, with points taken through the pool (head, trough and exit slope), as well as the upstream and downstream riffles. This compares with a dominance of points taken on riffles at the 3·6 $m^3$ $s^{-1}$ flow, due to difficulties taking measurements from the pool at this flow.

Simulated water depths, derived from subtracting the modelled water surface from a digital elevation model (DEM) of the bed, were compared with depths measured at points A–P (Figure 3b). Water depths for points A–P (Figure 3b) for four different model runs and the difference between calculated and observed depths are shown in Table IV. Water depth increases as bank roughness increases. Using a bank roughness value of 0·1 m was found to produce the lowest difference between measured and predicted water depths on average, and was therefore employed in the rest of the simulations in this paper. This value compares to a bed $D_{84}$ ranging from 0·092 to 0·195 m within the study reach.

Simulated depths at positions K (0·40 m) and L (0·64 m) are in the order of 0·3 m greater than those measured at these points (K = 0·10 m; L = 0·34 m). This difference may reflect survey error and error in the DEMs of the bed and water surface used to retrieve the simulated depth data. Survey accuracy was in the order of 0·01 m + 1 ppm in the horizontal and 0·02 m + 2 ppm in the vertical. DEM error tends to be greatest where there is high local topographic roughness, for example at bank or bar edges, and least on flatter surfaces such as bar tops (Heritage *et al.*, 2009). Spatial variability in error for both the bed and water surface DEMs was assessed through predicting local survey error

**Table IV.** Bank roughness calibration, through comparison of measured and simulated water depths (in metres) for the 1·52 $m^3 s^{-1}$ flow

| Position | Measured Depth (m) | Sim 0·1 | Diff 0·1 | Sim 0·2 | Diff 0·2 | Sim 0·5 | Diff 0·5 | Sim 0·75 | Diff 0·75 |
|---|---|---|---|---|---|---|---|---|---|
| A | 0·28 | 0·30 | 0·02 | 0·50 | 0·22 | 0·31 | 0·03 | 0·31 | 0·03 |
| B | 0·50 | 0·28 | −0·22 | 0·39 | −0·11 | 0·35 | −0·15 | 0·35 | −0·15 |
| C | 0·82 | 0·88 | 0·06 | 0·99 | 0·17 | 0·94 | 0·12 | 0·94 | 0·12 |
| D | 0·48 | 0·41 | −0·07 | 0·53 | 0·05 | 0·47 | −0·01 | 0·47 | −0·01 |
| E | 0·24 | 0·24 | 0·00 | 0·34 | 0·10 | 0·30 | 0·06 | 0·30 | 0·06 |
| F | 0·45 | 0·39 | −0·06 | 0·51 | 0·06 | 0·44 | −0·01 | 0·44 | −0·01 |
| G | 0·83 | 0·72 | −0·11 | 0·83 | 0·00 | 0·78 | −0·05 | 0·78 | −0·05 |
| H | 1·06 | 0·91 | −0·15 | 1·02 | −0·04 | 0·96 | −0·10 | 0·96 | −0·10 |
| I | 0·33 | 0·45 | 0·12 | 0·61 | 0·28 | 0·49 | 0·16 | 0·49 | 0·16 |
| J | 0·15 | 0·26 | 0·11 | 0·11 | −0·04 | 0·33 | 0·18 | 0·33 | 0·18 |
| K | 0·09 | 0·38 | 0·29 | 0·19 | 0·10 | 0·45 | 0·36 | 0·45 | 0·36 |
| L | 0·34 | 0·64 | 0·30 | 0·47 | 0·13 | 0·71 | 0·37 | 0·71 | 0·37 |
| M | 0·22 | 0·32 | 0·10 | 0·25 | 0·03 | 0·39 | 0·17 | 0·39 | 0·17 |
| N | 0·44 | 0·36 | −0·08 | 0·25 | −0·19 | 0·43 | −0·01 | 0·43 | −0·01 |
| O | 0·11 | 0·25 | 0·14 | 0·20 | 0·09 | 0·31 | 0·20 | 0·31 | 0·20 |
| P | 0·12 | 0·12 | 0·00 | 0·17 | 0·05 | 0·18 | 0·06 | 0·18 | 0·06 |
| Average | 0·40 | | 0·03 | | 0·06 | | 0·09 | | 0·09 |

Simulated (Sim) and the difference between simulated and measured depths (Diff) are shown for bank roughness values of 0·1 m, 0·2 m, 0·5 m and 0·75 m. Horizontal accuracy: 0·01 m + 1 ppm; vertical accuracy: 0·02 m + 2 ppm.

(difference between measured points and the DEM), from local topographic roughness (see Milan *et al.*, 2011), and then calculating the root mean square error. Vertical errors of 0·05 and 0·03 m were found at points K and L, respectively. Further error may have been introduced when recording the actual depth at these points due to (i) the bed shelving away from a bar (Figure 3b), and (ii) local variability in clast and local water surface roughness (for example unbroken standing waves compared with a flat water surface). However, the average difference between measured and predicted water depths was within the reach $D_{84}$. The bank roughness value of 0·1 was used simulate water depths at the 3·6 $m^3 s^{-1}$ flow, as an independent test of the roughness parameter (Table V). Although, depths are under-predicted on this occasion, the magnitude of the difference was similar to the 1·52 $m^3 s^{-1}$ simulation.

## Model validation

Model validation was conducted for 1·52 $m^3 s^{-1}$ and 3·6 $m^3 s^{-1}$. These were the only two events that could be captured safely for detailed velocity measurements, without the need for platforms or structures mounted over the pool. Flows of up to 11·9 $m^3 s^{-1}$ were simulated in this investigation, well outside the validation discharges, hence some caution needs to be given when interpreting the output. A comparison of simulated and measured velocities taken at both validation discharges is shown in Figure 5, where the line shown is that for one-to-one agreement. The locations of the velocity measurements, taken using a Marsh McBirney flow meter are shown in Figures 3b and 3c. For the 1·52 $m^3 s^{-1}$ flow, velocities were measured at 0·1, 0·2, 0·6, 0·8 flow depth where depth permitted. For the 3·6 $m^3 s^{-1}$ flow, velocities were measured at 0·1, 0·2 and 0·4 of the flow depth. Although there is some scatter, data plots around the one-to-one lines for both the 1·52 $m^3 s^{-1}$ and 3·6 $m^3 s^{-1}$ flows. For the 1·52 $m^3 s^{-1}$ flow greatest deviation from the 1:1 line is shown for points H, M, I and K. Points H and I are both situated close to the bank at the outer edge of the meander before the deepest part of the pool (Figure 3b). Point M is situated on the riffle downstream. Point K is situated on the edge of the lateral bar further downstream, and may experience secondary flow. For the 1·52 $m^3 s^{-1}$ simulation, linear regression yielded

**Table V.** Comparison of measured and simulated water depths (in metres) for the 3·6 $m^3 s^{-1}$ flow, using a bank roughness value of 0·1 m

| Position | Measured | Predicted | Difference |
|---|---|---|---|
| A | 0·92 | 0·91 | 0·01 |
| B | 0·98 | 1·00 | −0·02 |
| C | 1·05 | 1·03 | 0·02 |
| D | 0·28 | 0·26 | 0·02 |
| E | 0·38 | 0·37 | 0·01 |
| F | 0·46 | 0·36 | 0·10 |
| G | 0·29 | 0·37 | −0·08 |
| H | 0·42 | 0·40 | 0·02 |
| I | 0·46 | 0·36 | 0·10 |
| J | 0·3 | 0·51 | −0·21 |
| K | 0·42 | 0·43 | −0·01 |
| L | 0·35 | 0·34 | 0·01 |
| M | 0·34 | 0·61 | −0·27 |
| N | 0·34 | 0·44 | −0·10 |
| O | 0·25 | 0·33 | −0·08 |
| P | 0·44 | 0·53 | −0·09 |
| Q | 0·5 | 0·46 | 0·04 |
| R | 0·34 | 0·35 | −0·01 |
| S | 0·49 | 0·76 | −0·27 |
| T | 0·55 | 0·52 | 0·03 |
| U | 0·44 | 0·36 | 0·08 |
| V | 0·53 | 0·86 | −0·33 |
| W | 0·64 | 0·61 | 0·03 |
| X | 0·36 | 0·40 | −0·04 |
| Y | 1·01 | 0·97 | 0·04 |
| Z | 0·82 | 0·99 | −0·17 |
| a | 1·08 | 0·99 | 0·09 |
| Mean | | | −0·04 |

$$U_{sim} = 0.865 U_{obs} + 0.057 \quad (8)$$

with an $r^2$ value of 0·56 (sample size 60), where $U_{sim}$ and $U_{obs}$ are the simulated and observed velocities, respectively. For the 3·6 $m^3 s^{-1}$ simulation, linear regression yielded

$$U_{sim} = 1.051 U_{obs} - 0.045 \quad (9)$$

with an $r^2$ value of 0·51 (sample size 81). To provide a better picture of model performance, and to check for bias in these relationships, a standardized major axis regression (Warton *et al.*, 2006) was applied to all two sets of data to test for significant

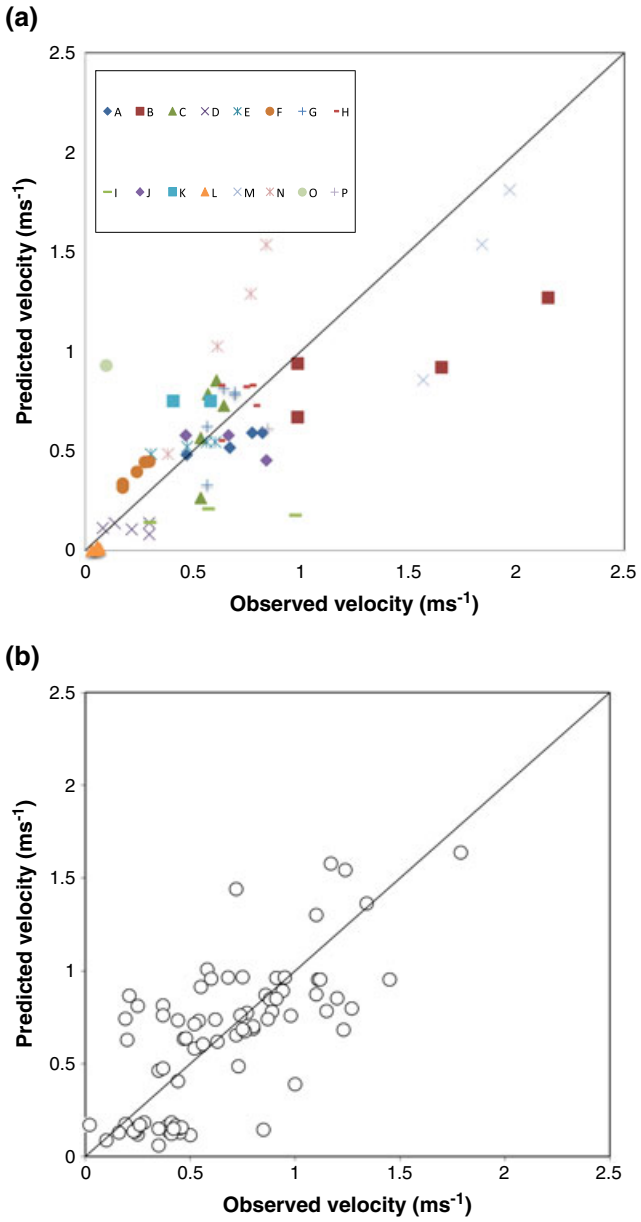


**Figure 5.** Comparison of measured versus simulated streamwise velocity, for the (a) $1 \cdot 52$ m$^3$ s$^{-1}$ and (b) $3 \cdot 6$ m$^3$ s$^{-1}$ runs. The 1:1 line is indicated. This figure is available in colour online at wileyonlinelibrary.com/journal/espl

differences between a slope of one and an intercept of zero. Thus $p$ values were both in excess of $0 \cdot 05$ indicating no significant differences for slope and intercept values for the $1 \cdot 52$ m$^3$ s$^{-1}$ and $3 \cdot 6$ m$^3$ s$^{-1}$ runs.

# Results

## Clast tracers

Tracer recovery declined from 92% following the first event to 65% at the end of the 18 month study duration (Table VI). This is comparable to other studies using PITs embedded in clasts (e.g. Lamarre and Roy, 2008), and is a substantial improvement to earlier work conducted on the same study reach on the Rede using painted clasts without PITs that showed a recovery rate of only 21% after a 13 month period (Milan *et al.*, 2002).

To provide an indication of clast pathways relative to pool-riffle morphology, pre- and post-flood tracer loci for three different size classes (20–70 mm, 70–100 mm, and 100–200 mm) connected with a straight line for eight flood events between November 2005 and May 2008, are draped over a DEM of the pool-riffle unit (Figure 6). Greatest movement was shown during the first flood event (7.8 m$^3$ s$^{-1}$), partly due to the overloose nature of the tracers; all tracers were initially located on the bed surface rather than in buried or structured positions. Greatest movement is shown for the 20–70 mm size class following this event. There is a clear tendency for all clasts, regardless of size, to be routed onto and deposited on the point bar rather than being routed through the thalweg towards the pool. A 70–100 mm clast seeded in the trough of the pool was ejected out of the pool onto a downstream bar, whilst three 100–200 mm clasts in the trough of the pool were transported onto the pool exit slope. Event 2 also resulted in some tracer movement from the upstream riffle onto the bar. Little movement is shown after events 3 and 4. Tracer clasts between 20 and 100 mm were transported from the upstream bar edge to the downstream riffle after event 5. Significant movement is also shown following events 7 and 8. During these two events, clasts were transported onto the bar, there was movement of clasts on the bar towards the riffle, and some clasts were scoured out of the pool trough on to the pool exit slope or the downstream riffle or bar. Very few clasts were found to be transported into the pool (Table VI). Single clasts in the 20–70 mm size fraction were found in the pool following events 3 and 5, and two clasts were found following event 7. No clasts in the 70–100 mm size class were found to be deposited in the pool. Single clasts in the 100–200 mm size class were found to be deposited in the pool following events 1 and 2. There was no significant difference in the routing of clasts by grain-size (chi square test: chi square = $0 \cdot 098$, $p > 0 \cdot 05$). Although these data are limited to a knowledge of tracer start and end position, tracer data strongly suggest that clasts tend not to be routed towards the pool at any flow stage. Occasional clasts that were found in the pool (Table VI) are likely to have been routed across the bar surface, and then rolled down the avalanche face into the pool (*sensu* Dietrich and Smith, 1984).

**Table VI.** Tracer statistics over following eight resurveys between 5 November 2006 and 11 May 2008.

| | | | 20–70 mm | | 70–100 mm | | 100–200 mm | |
|---|---|---|---|---|---|---|---|---|
| Event | Percentage recovery | Proportion transported > 0 · 2m | Total clasts retrieved | Proportion avoiding pool | Total clasts retrieved | Proportion avoiding pool | Total clasts retrieved | Proportion avoiding pool |
| 1 | 92 | 87 | 33 | 100 | 31 | 100 | 25 | 96 |
| 2 | 89 | 45 | 33 | 100 | 29 | 100 | 24 | 96 |
| 3 | 86 | 40 | 31 | 97 | 27 | 100 | 25 | 100 |
| 4 | 83 | 65 | 30 | 100 | 28 | 100 | 23 | 100 |
| 5 | 43 | 88 | 14 | 93 | 14 | 100 | 13 | 100 |
| 6 | 69 | 88 | 28 | 100 | 21 | 100 | 19 | 100 |
| 7 | 70 | 90 | 24 | 92 | 22 | 100 | 21 | 100 |
| 8 | 65 | 94 | 21 | 100 | 23 | 100 | 20 | 100 |

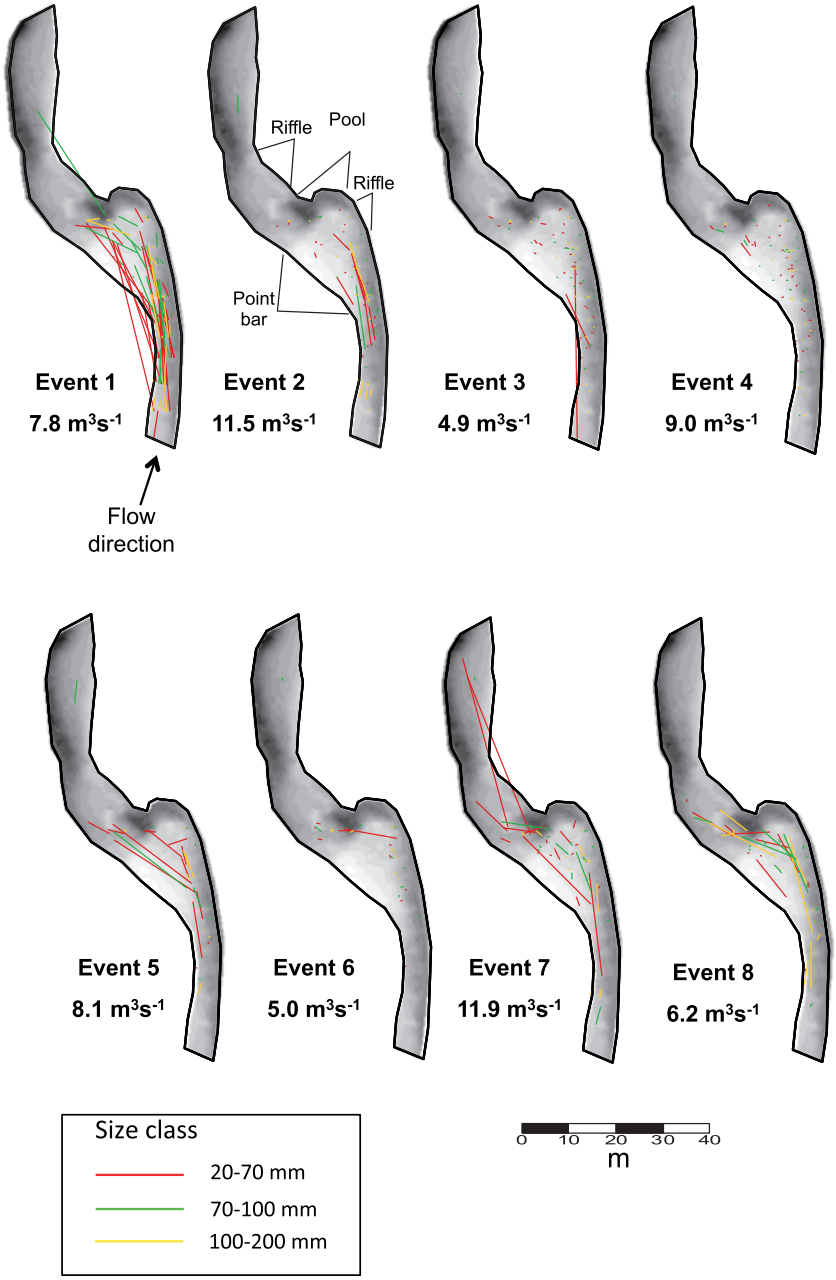


**Figure 6.** Tracer clast pathways following eight re-surveys between 5 November 2006 and 11 May 2008. Start and end loci for individual clasts have been linked with a straight line. This figure is available in colour online at wileyonlinelibrary.com/journal/espl

## Sediment transport

Continuous sediment transport (load cell) data for the four bedload traps situated throughout the pool-riffle unit, for a sequence of five flood events between 7–15 January 2007, are demonstrated in Figure 7. Flood magnitude over this period ranged between 4 and $11 \cdot 5$ m$^3$ s$^{-1}$ (over bank flow). Sediment appears to be transported out of the pool during the first flood in the series late on the 7 January (4 m$^3$ s$^{-1}$), however no sediment enters the traps situated on the upstream riffle and the pool entrance indicating that sediment is not being routed into the pool. During the second event in the series (7 m$^3$ s$^{-1}$), the upstream riffle, pool exit and downstream riffle traps are all active, with greatest sediment transport rate appearing on the downstream riffle and the lowest appearing for the upstream riffle. The third and largest event in the series ($11 \cdot 5$ m$^3$ s$^{-1}$) demonstrates the largest (and similar) bedload transport rates for the upstream and the downstream riffles, whilst intermediate sediment transport rates are found at the pool exit slope. The bedload trap situated at the pool entrance for the first time shows a response, possibly indicating a small amount of sediment transport in this region, although the data here is indistinguishable from noise in the data trace.

The trap situated at the pool entrance consistently filled with the least amount of sediment, and often this would comprise of only sand, whilst other traps would fill with gravel. On the occasions where the trap did contain gravel, the clasts were clearly derived from within a close vicinity of the trap as they were still algae-covered; a characteristic of immobile clasts located in the pool on the outside of the bend. Drops in the order of 10 kg shown in phase with the secondary flood peak found on the falling limb of the larger peak, on the afternoon of 11 January, may represent remobilization of sediment covering the top of the trap, which was occasionally observed. The fourth flood peak ($5 \cdot 5$ m$^3$ s$^{-1}$) on the afternoon of 12 January appears to mobilize a small amount of bedload from the pool towards the pool exit slope trap. The last flood in the series indicates the downstream riffle to be transporting the most sediment, with some deposition

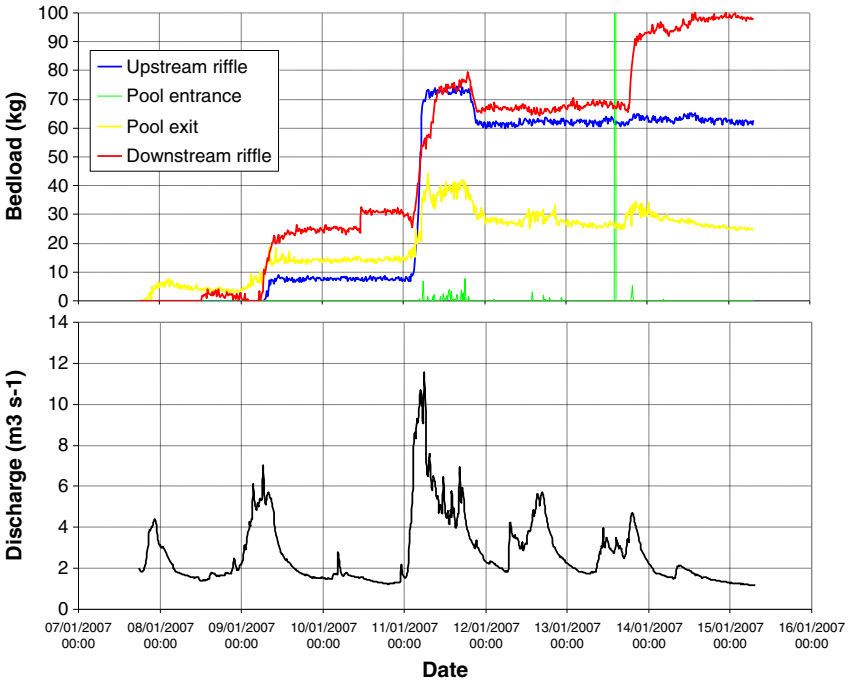


**Figure 7.** Sediment transport series for four bedload traps situated in different positions along the thalweg through the pool-riffle sequence, for the period 7–15 January 2007. The trace in the figure shows cumulative sediment accumulation of the time period. This figure is available in colour online at wileyonlinelibrary.com/journal/espl

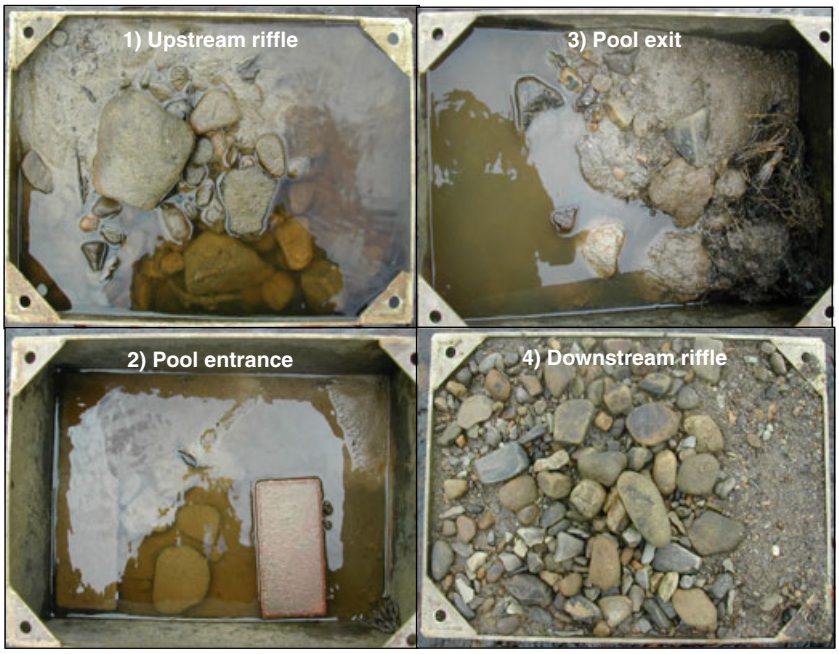


**Figure 8.** Material collected in the four bedload traps after the sequence of events shown in Figure 7, between 7-15 January 2007. Photographs taken on 15 January 2007. Grain-size and sorting differences are visually evident between the traps. Trap 1 on the riffle upstream of the pool contains a very poorly sorted deposit with a high sand content and coarse cobbles, with very little medium gravel. Pool entrance trap 2 has captured very little sediment indicating negligible sediment routing through this part of the channel. The brick which is visible in trap 2 was used to apply an initial load to the load cell. There is a very high sand content with occasional cobbles and bank material captured in trap 3 on the pool exit slope, whilst the downstream riffle (trap 4) has collected medium gravel with a low sand content. This figure is available in colour online at wileyonlinelibrary.com/journal/espl

**Table VII.** Mean and range (in brackets) weight, grain size, sorting and skewness data for material collected in bedload traps on eight separate occasions between 1st Nov 2005 and 3rd Mar 2007. The sorting index used is the Graphic Standard Deviation ($\sigma_G$) (Folk, 1974), which measures the deviation of the 16th and 84th percentiles $\frac{(\varnothing 84-\varnothing 16)}{2}$

| Trap position | Weight (kg) | $D_{50}$ (mm) | Sorting | Skewness |
|---|---|---|---|---|
| **TRAP 1** Upstream riffle | 91 (8-157) | 17.7 *(0.5-30.0)* | 2.1 *(0.4-3.0)* | 1.2 *(0.3-5.2)* |
| **TRAP 2** Pool entrance | 7 (0-20) | 18.6 *(0.5-56.0)* | 2.9 *(0.4-5.0)* | 2.0 *(0.2-5.2)* |
| **TRAP 3** Pool exit | 64 (0-157) | 9.7 *(0.7-23.0)* | 2.3 *(0.5-4.4)* | 1.2 *(0.3-4.2)* |
| **TRAP 4** Downstream riffle | 81 (0-157) | 10.9 *(1.9-30.5)* | 2.6 *(1.2-3.4)* | 0.8 *(0.2-3.0)* |

on the pool exit slope trap. The upstream riffle and the pool entrance both appear inactive. The large peak occurring on the afternoon of 13 January for the pool entrance trap is likely to be due to noise in the data, as this is short lived and does not relate to discharge peaks.

## Sediment grain-size and sorting

Figure 8 demonstrates the material that accumulated in the traps following the flood series shown in Figure 7, whilst Table VII demonstrates the mean and range of grain size information ($D_{50}$, sorting and skewness) for samples taken from a longer time period; over eight different events between 1 November 2005 and 3 March 2007. For sediment accumulating between 7-15 January 2007 it can be seen that the upstream riffle trap contains a large quantity of sand, with occasional coarse gravel clasts. The fine sediment fraction caught in this trap consistently had a very high organic content, and was dominated by fine sands and silts. The fine sediment captured in the other traps tended to comprise of medium-coarse sand. The pool entrance trap contained very little sediment. This trap consistently recorded the lowest weights over the full study duration (Table VII). Bricks, one of which can be seen in Figure 8, were

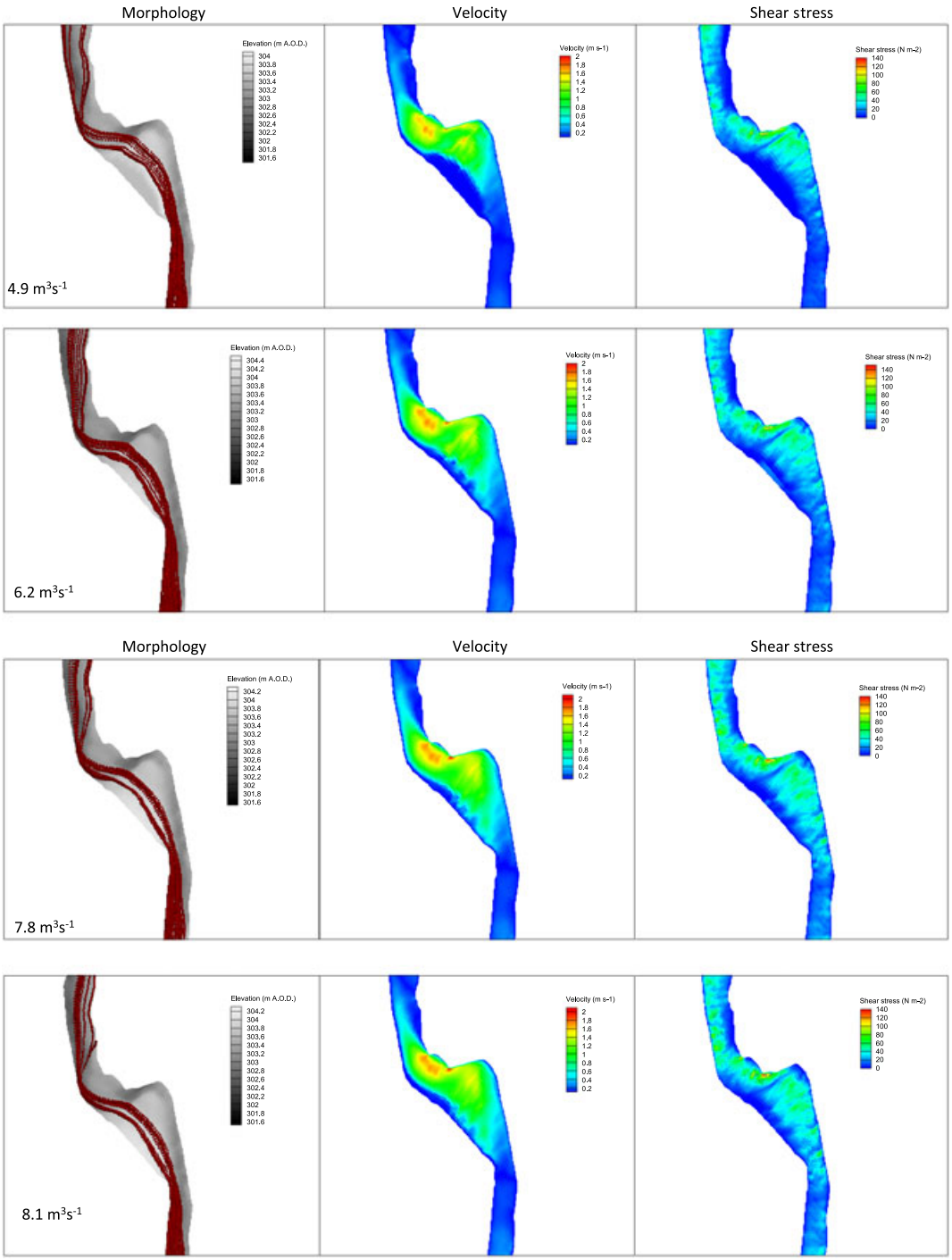


**Figure 9.** CFD results for $4 \cdot 9$ to $11 \cdot 9$ m$^3$ s$^{-1}$ simulations. Simulated flow trajectories draped over bed morphology DEM, streamwise ($x$) velocity and boundary shear stress, for seven out of the eight events responsible for transporting tracer clasts. Origin of streamlines located in each cell of the computation mesh at the head of the reach upstream, and across the full width of channel (Figure 4b). This figure is available in colour online at wileyonlinelibrary.com/journal/espl

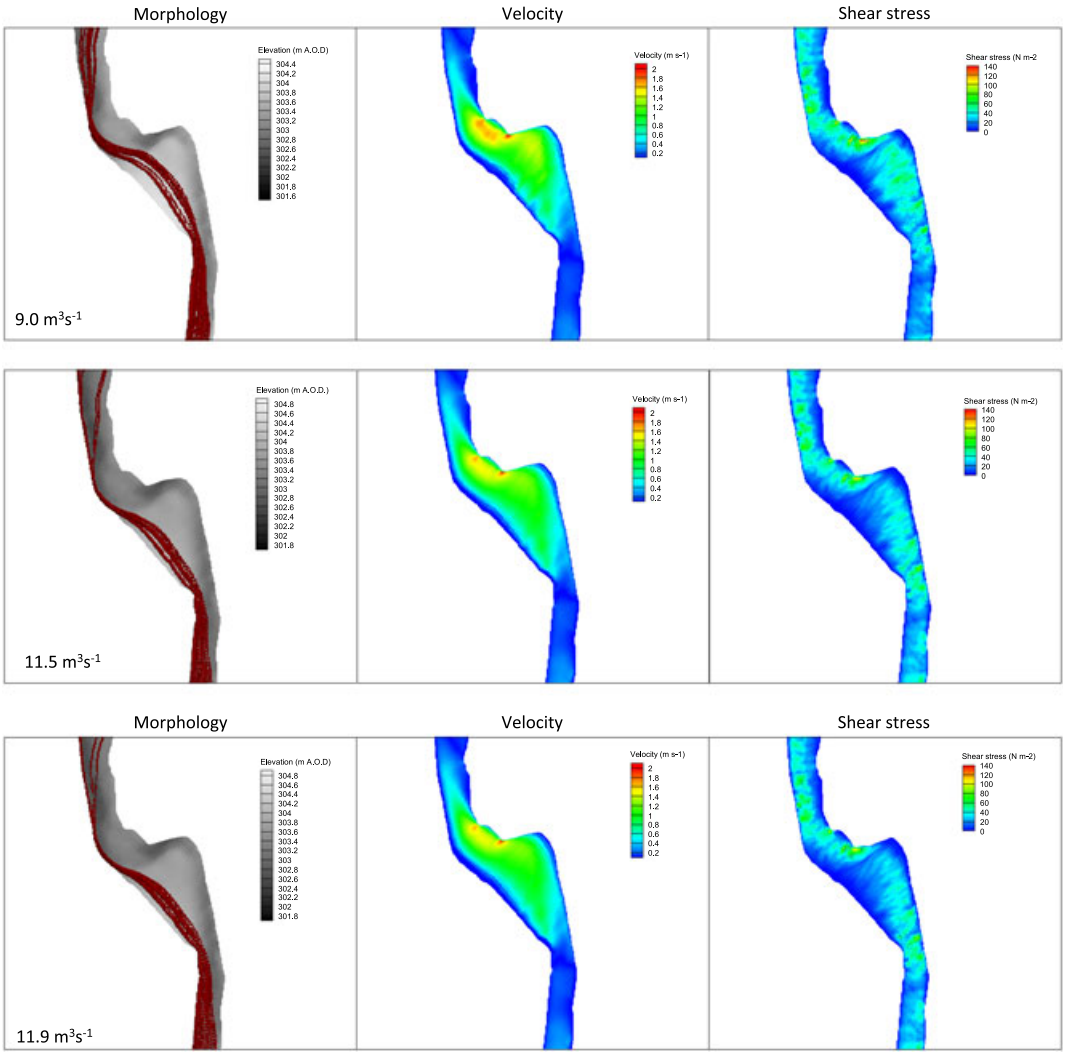


**Figure 9.** Continued.

used to apply an initial load to the load cell in each trap, in order for any additional load to be detected. The small quantity of material that had accumulated was sand, with occasional locally derived coarse gravel, resulting in the poorest sorting and most skewed grain size distribution (Table VII). Fine and medium gravel never accumulated in this trap over the study duration. The pool exit slope trap contains a large quantity of sand with medium gravel. Overall this trap collected the finest sediments over the study duration (Table VII). Also noticeable is the significant amount of bank material (soil and organics) caught in this trap. Bank-derived material was found on a number of occasions in this trap, and was often deposited as spherical chunks of cohesive material, rounded by transport along the bed. This suggested that sediment was sourced locally from an upstream eroding outer bank adjacent to the pool. The downstream riffle trap collected the most material in the gravel size range following this flood series (Figure 8).

In summary, both tracer and trap data appear to suggest no sediment transport into pools along the thalweg. Instead material is routed over the point bar surface, or along the edges on the point bar. CFD was used to further explore the hydraulics responsible for the observed sediment movement.

## CFD findings

Steady-state CFD simulations were run for seven of the eight flows responsible for tracer movement. Figure 9 illustrates maps of bed morphology, patterns of near-bed velocity and shear stress for the range of flows considered. Velocity trajectories (streamlines) calculated using a streamline function that interpolates near-bed flow vectors in the bottom cell of the computational mesh (< 7% of the flow depth from the bed), were draped over these. Streamlines indicate the path taken by a massless particle in a steady-state vector field, with the start point positioned in each near bed cell at the entrance cross-section of the model domain. Local shear stress maxima have a tendency to be located in a small zone towards the outer bank of the pool. Velocity maxima are also found in this location, however a larger area of high velocity is a feature across the downstream riffle for most of the discharges considered, although there are some subtle variations. Low shear stresses tend to be found just upstream of the pool towards the bend apex for the higher flow simulations ($> 7 \cdot 8$ m$^3$ s$^{-1}$), and also on the inside of the bar throughout the flow range. For the reach as a whole, shear stress and velocity maxima appeared to occur just below bankfull discharge for the $7 \cdot 8$ to $9 \cdot 0$ m$^3$ s$^{-1}$ flows, rather than the peak discharges. A reduction in velocity appears to be a feature over the downstream riffle for flows in excess of 11 m$^3$ s$^{-1}$. For the $4 \cdot 9$ and $6 \cdot 2$ m$^3$ s$^{-1}$ simulations, shear stress is high towards the centre of the bar and the bar edge. This area of high shear stress extends further upstream for the $7 \cdot 8$ and $8 \cdot 1$ m$^3$ s$^{-1}$ flows. Whereas for the $11 \cdot 5$ and $11 \cdot 9$ m$^3$ s$^{-1}$ simulations the bar head exhibits greater shear stresses compared with the middle and tail of the bar.

Simulated flow trajectories strongly support the observed tracer clast pathways. For each of the flows considered,

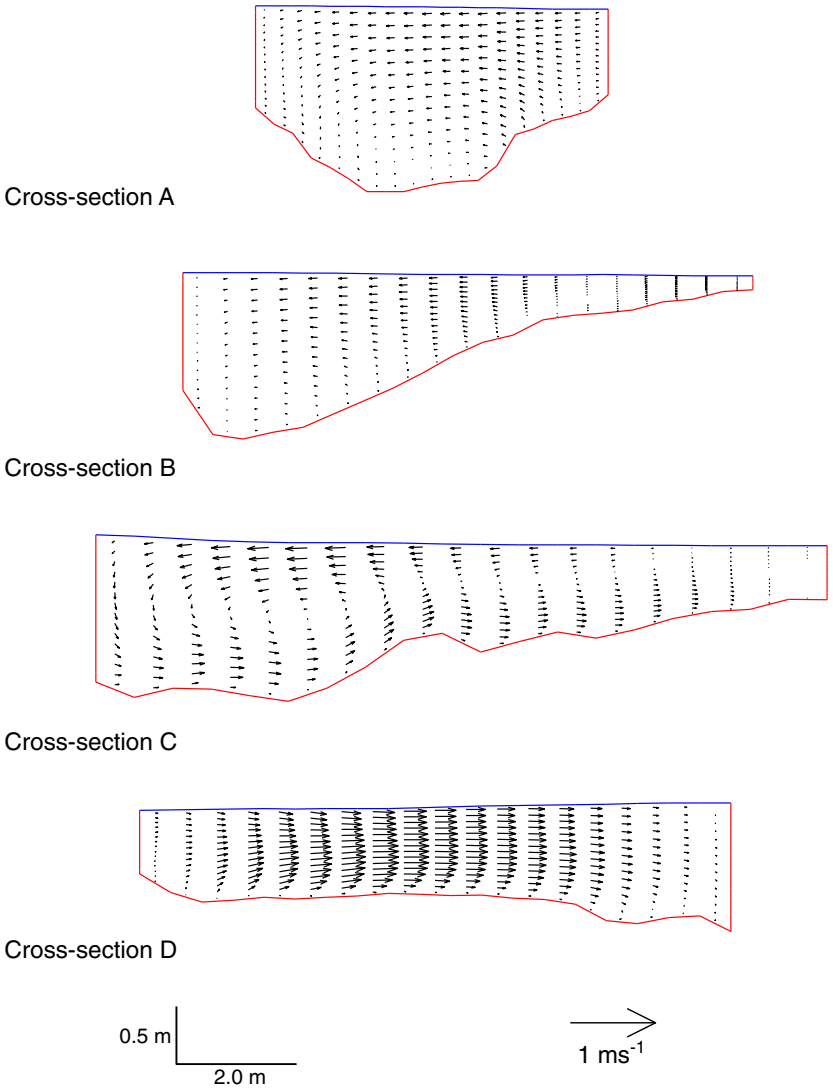


**Figure 10.** Simulated secondary flow vectors for four cross-sections taken through the Rede pool-riffle unit for a discharge of $8 \cdot 1$ m$^3$ s$^{-1}$. The position of the cross-sections are indicated in Figure 3a. This figure is available in colour online at wileyonlinelibrary.com/journal/espl

velocity trajectories show strong convergence towards the shallower left-hand side of the channel towards the point bar head. Flow trajectories appeared to avoid areas of highest velocity and shear stress, and clearly steer away from the thalweg for all simulated flows. For all the simulations flow trajectories are clearly routed over the bar surface, rather than being routed around the thalweg towards the outer bank. For the lower discharges ($4 \cdot 9$ and $6 \cdot 2$ m$^3$ s$^{-1}$) flow trajectories split into two main ribbons; with one that hugs the inside of the bar top, and a second that feeds into the left hand side of the pool, down the avalanche face of the point bar tail. The two ribbons are also a feature of the $7 \cdot 8$ and $8 \cdot 1$ m$^3$ s$^{-1}$ simulations, although the outer ribbon appears to skirt round the avalanche face of the point bar, avoiding the pool trough. These findings would further support the notion that sediment is not routed into the pool.

### Cross-sectional flow patterns

Weak secondary circulations are evident for the pool entrance and pool trough cross-sections (B and C), shown in Figure 10 for the $8 \cdot 1$ m$^3$ s$^{-1}$ simulation. The pool entrance section indicates weak outward surface velocities and downwelling towards the outer bank, that is likely to promote bank erosion. The pool trough cross-section (C) indicates a well-developed cross-stream rotational eddy, with surface flow towards the outer bank, downwelling at the outer bank, and upwelling, and near-bed flow vectors directing flow inwards towards the point bar. These near bed flow vectors are likely to promote bar edge deposition of fine sediment. These cross-sectional flow patterns were also a feature shown in the other simulations.

## Discussion

### Sediment Sorting through the Pool-Riffle Unit

Conventional notions of sediment routing along with the hydraulic reversal model (Figure 1) are thought to be responsible for the observed variations in sorting of the surface layer of sediments between pools and riffles, with riffles being most commonly reported as being coarser and better sorted than pools (Table I). A number of studies (e.g. Clifford, 1990) suggest that if pools exhibit higher tractive forces at peak flows in comparison to adjacent riffles, then they should be competent to transport every grain size that is fed into them, importantly including the coarsest gravels within the system. Hence at peak flows, gravel is stranded on the relatively lower competence riffles. Under lower flows, not capable of transporting gravel, fines are then selectively transported off the riffles and routed into the pools, and stored until the next high flow event.

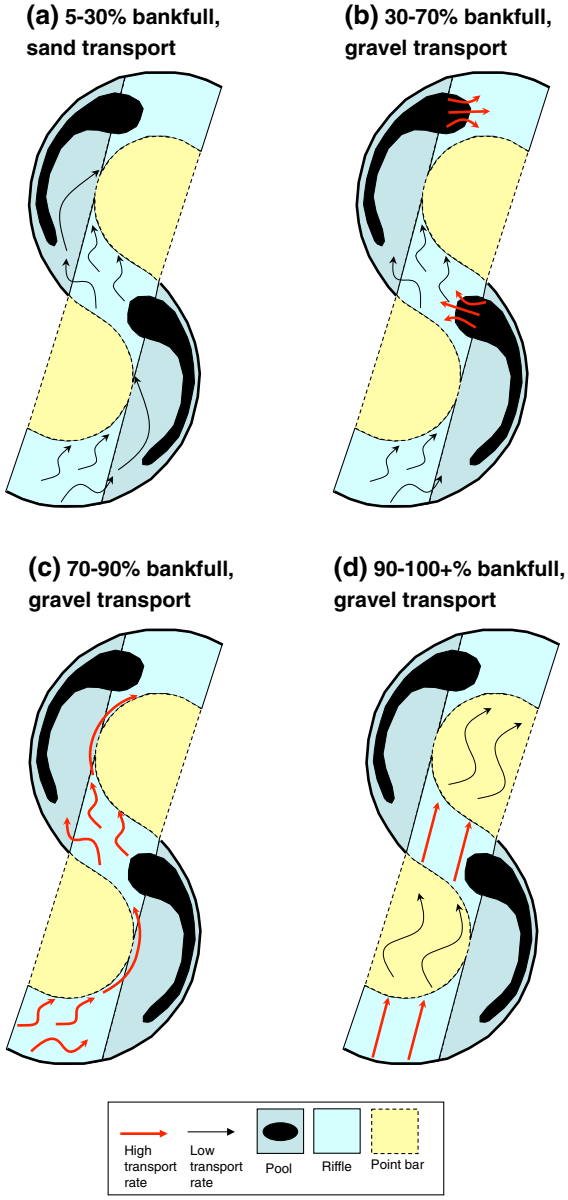


**Figure 11.** Revised sediment routing model, where sediment is predominantly routed onto bars rather than through pool, allowing pool maintenance without hydraulic reversal. This figure is available in colour online at wileyonlinelibrary.com/journal/espl

Several studies have reported coarse sediments in pools (e.g. Gilbert, 1914; Ashworth, 1987), most of which suggest that these are lag deposits derived from erosion of bank material or scour into till (Keller, 1982). This has also been suggested by Leopold *et al.* (1964) to explain some of Hack's (1957) results. Bhowmik and Demissie (1982) and Thompson *et al.* (1999) contend that the coarsest bed material should be found in the pool troughs as pools represent zones of maximum competence. Carling and Wood's (1994) one-dimensional modelling suggests that coarser pools may promote the likelihood hydraulic reversal.

As grain size character is most commonly observed at low flow, the grain size patterns recorded by most investigators tend to reflect a range of flow and sediment supply scenarios. Some studies have highlighted the difficulty in gaining reliable grain size data particularly for pools (Richards, 1976a; Carling, 1991), and some of the data published in many past studies (Table I) may include information on low flow deposits or an unrepresentative mixture of high and low flow materials. Pools in gravel-bed streams with a high fine sediment supply, may exhibit low grain roughness at low flow as the fine sediment covers the gravels beneath. However, during a flood event the fine sediment may be flushed from the pool revealing a hydraulically rough bed at high flow (*sensu* Lisle, 1979).

The role of fine sediment supply in determining the observed low flow grain size has been shown to be significant (e.g. Lisle and Hilton, 1992). In streams with a high supply of fines, material deposited on riffles during high flow is selectively winnowed into the less competent pools on the falling limb of the hydrograph where it is stored until the next high flow event. In supply-limited streams, such as the Rede, the quantity of fines stored in pools is considerably reduced, hence the high flow sorting patterns are easier to observe and are not disguised by low flow deposits. Bhowmik and Demissie (1982) claim low flow winnowing to be a primary factor responsible for the reported sorting differences between riffles and pools, rather than high flow velocity reversal as suggested by Keller (1971).

## Sediment routing model of pool-riffle maintenance

The data presented in this study on gravel transport and flow hydraulics, in conjunction with existing knowledge on gravel pathways and sand transport within the reach (see Milan, 2000; Milan *et al.*, 2002) allows a revision of the conceptual model presented in Figure 1, this time accounting for stage-dependent sediment and flow routing patterns (Figure 11). Sand is stored mainly on bar tails and riffle margins, with no sediment storage in pools, contrasting to some previous studies (e.g. Lisle, 1979; Lisle and Hilton, 1992). At low flows up to around 30% bankfull before the gravel armour is disrupted, sand transport can take place if there is supply on the riffle surface. This will have a tendency to be routed towards the bar head. Any fines routed towards the pool are likely to be deflected towards the bar edge by secondary flows (Figure 10; Bathurst *et al.*, 1979; Dietrich and Smith, 1984). At flows between 30 and 70% bankfull, shear stresses in the pool head and trough are capable of transporting gravels. The coarse pool bed acts as a protective lag, limiting further vertical scour (Milan, 2000). At these flow stages, most sediment is derived from bank scour (trap 3; Figure 8). This material is fed downstream and dumped on the pool exit slope. At between 70 and 90% bankfull, prior to full bar surface submergence, clasts are routed around the edges of bars. Clasts may fall down the leading avalanche face of the bar, and get fed into the pool trough at this stage, similar to Dietrich and Smith (1984). At between 90 and >100% bankfull clasts are transported directly onto the bar surface, and get transported along the inside edge of the bar. At this flow stage these clasts may miss the avalanche face of the bar, avoid the pool, and get fed directly onto the downstream riffle. At this bankfull flow stage sediment transport takes a much more direct pathway, with the pools effectively becoming redundant in terms of sediment transfer from upstream. Here, riffles are effectively behaving as the pools and the bar tops are behaving as the riffles (*sensu* Hey, 1982), as the riffles have comparatively lower elevation and greater tractive force in comparison to the bar top. On the falling limb of the hydrograph both coarse and fine sediment may be deposited on the bar surface, with some preferential transport of fines towards the bar tail.

The findings presented in this study have similarities to Dietrich and Smith's (1984) work on Muddy Creek, in that the point bar appears to the zone of maximum sediment transport. However their work strongly suggests routing of sediment into the pool (Dietrich and Smith, 1984, p. 1370), contrasting with the findings in this investigation. On the Rede, secondary circulations are most likely to be too weak to deflect coarse clasts inward if any

clasts were to be fed into the pool, but may be sufficient to halt clasts that are fed over the bar top toward the bar edge. However, very few clasts ever appeared to be transported into positions where they may fall into the pool. Clast pathways appear to follow streamlines, that have a tendency to track along the inside of the point bar and avoid the pool, and hence appear to be controlled by near-bed velocity vector direction.

There is a need for more work to test how widely applicable pool avoidance of clasts is. Keller and Florsheim (1993) were able to demonstrate that the velocity reversal hypothesis was valid for a straight pool-riffle sequence on Dry Creek, however acknowledge that more complex hydraulics and sediment transport processes, such as those alluded to in Dietrich *et al.*'s (1979) work on Muddy Creek, may result in alternative pool-riffle maintenance mechanisms in meandering channels. The degree of channel sinuosity therefore could be an important control upon the dominant pool-riffle maintenance mechanism. Furthermore, the position of the pool trough relative to the point-bar morphology also appears to be important. In situations where the pool is channel wide and the channel is straight, clasts are likely to be routed through the pool. However, pool avoidance by clasts may be more likely where the pool cross-section has strong asymmetry and where the planform is sinuous or meandering.

## Conclusions

1. On the River Rede pool head maintenance occurs both through clast routing which diverts material (delivered from upstream) away from the pool over the point-bar surface, and through hydraulic maintenance, where material that is eroded from the outer bank is flushed towards the pool exit slope downstream.
2. Sediment routing appears to show a strong linkage with flow trajectories and is not necessarily linked to areas of peak tractive force.
3. High tractive forces do appear to be important for maintaining the pool trough, through flushing out bed material delivered from (i) across the bar surface and down the leading avalanche face of the bar, and (ii) bank erosion, rather than material delivered along the thalweg as is conventionally assumed.
4. The conventional model of sediment transport into pool troughs (Figure 1) does not apply to the Rede pool-riffle sequence. Lower flow (winnowing) of fines into the pool (*sensu* Lisle, 1979; Lisle and Hilton, 1992) does not occur, as during these lower flows (0–30% bankfull) fines are routed onto shallow riffle margins or pool heads. Gravel does not get routed into the pool at medium flows either, as sediment is not being routed along the thalweg. Sediment delivery to the pool from upstream requires bar submergence; on the Rede flows of 70 to 90% bankfull are necessary for this to be achieved, however very few clasts were deposited in the pool. At bankfull discharge and above, flow trajectories and associated clast pathways avoid the pool altogether.

In conclusion it is possible that pool-riffle maintenance can be explained through sediment routing processes, without recourse to the hydraulic reversal mechanism. River restoration schemes aimed at reinstating pool-riffle morphology should therefore consider this mode of maintenance in addition to other models.

*Acknowledgements*—The British Society for Geomorphology kindly supported purchase of the PIT kit, through the award of a research grant to the author. The author also acknowledges the constructive comments of Ed Keller, an anonymous referee and Stuart Lane.

## References

Andrews ED. 1979. *Scour and Fill in a Stream Channel*: *East Fork River, Western Wyoming*, US Geological Survey Professional Paper 1117. US Geological Survey: Reston, VA.

Andrews ED. 1983. Entrainment of gravel from naturally sorted river-bed material. *Geological Society of America Bulletin* **95**: 371–378.

Ashworth PJ. 1987. Bedload Transport and Channel Change in Gravel-bed Rivers, PhD Thesis, University of Stirling.

Bathurst JC, Thorne CT, Hey RD. 1979. Secondary flow and shear stress at river bends. *Journal of the Hydraulics Division, American Society of Civil Engineers* **14906**(HY10): 1277–1295.

Bhowmik NG, Demissie M. 1982. Bed material sorting in pools and riffles. *Journal of Hydraulic Engineering, American Society of Civil Engineers* **108**: 1227–1231.

Biron PM, Carver RB, Carre DM. 2011. Sediment transport and flow dynamics around a restored pool in a fish habitat rehabilitation project: field and 3D numerical modeling experiments. *River Research and Applications* **28**: 926–939.

Booker DJ. 2003. Hydraulic modelling of fish habitat in urban rivers during high flows. *Hydrological Processes* **17**: 577–599.

Booker DJ, Sear DA, Payne AI. 2001. Modelling three dimensional flow structures and patterns of boundary shear stress in a natural pool-riffle sequence. *Earth Surface Process and Landforms* **26**: 553–576.

Buffington JM, Lisle TE, Woodsmith RD, Hilton S. 2002. Controls on the size and occurrence of pools in coarse-grained forest rivers. *Rivers Research and Applications* **18**: 507–531.

Caamaño D, Goodwin P, Buffington JM. 2010. Flow structure through pool-riffle sequences and a conceptual model for their sustainability in gravel-bed rivers. *River Research and Applications* **28**: 377–389.

Carling PA. 1991. An appraisal of the velocity-reversal hypothesis for stable pool-riffle sequences in the River Severn, England. *Earth Surface Processes and Landforms* **16**: 19–31.

Carling PA, Wood N. 1994. Simulation of flow over pool-riffle topography: a consideration of the velocity reversal hypothesis. *Earth Surface Processes and Landforms* **19**: 319–332.

Cherkauer DS. 1973. Minimisation of power expenditure in a riffle-pool alluvial channel. *Water Resources Research* **9**: 1613–1628.

Church M. 1972. Baffin Island Sandurs: a study of Arctic fluvial processes *Canada Geological Survey Bulletin* **216**: 89–93.

Clifford NJ. 1990. *The Formation, Nature and Maintenance of Riffle-pool Sequences in Gravel-bedded Rivers*, Unpublished PhD Thesis, University of Cambridge.

Clifford NJ. 1993. Differential bed sedimentology and the maintenance of riffle-pool sequences. *Catena* **20**: 447–468.

Clifford NJ, Robert A, Richards KS. 1992. The reversal hypothesis and the maintenance of riffle-pool sequences: a review and field appraisal. In *Lowland Floodplain Rivers*: *Geomorphological Perspectives*, Carling PA, Petts GE (eds). John Wiley & Sons: Chichester; 43–70.

Clifford NJ, Richards KS. 1992. Estimation of flow resistance in gravel-bed rivers: a physical explanation of the multiplier of roughness length. *Hydrological Processes* **17**: 111–126.

Clifford NJ, Soar PJ, Harmar OP, Gurnell AM, Petts GE, Emery JC. 2005. Assessment of hydrodynamic simulation results for eco-hydraulic applications: a spatial semivariance approach. *Hydrological Processes* **19**: 3631–3648.

Clifford NJ, Wright, NG, Harvey G, Gurnell AM, Harmar OP, Soar PJ. 2010. Numerical modeling of river flow for ecohydraulic applications: some experiences with velocity characterization in field and simulated data. *Journal of Hydraulic Engineerin, American Society of Civil Engineers* **136**(12): 1033–1041.

Dietrich WE, Smith JD. 1984. Bedload transport in a river meander. *Water Resources Research* **20**: 1355–1380.

Dietrich WE, Smith JD, Dunne T. 1979. Flow and sediment transport in a sand bedded meander. *Journal of Geology* **87**: 305–315.

Emery JC, Gurnell AM, Clifford NJ, Petts GE, Morrissey IP, Soar PJ. 2003. Classifying the hydraulic performance of riffle-pool bedforms for habitat assessment and river rehabilitation design. *River Research and Applications* **19**: 533–549.

Folk RL. 1974. Petrology of sedimentary rocks. Hemphill: London.

Gilbert GK. 1914. *Transportation of Debris by Running Water*, US Geological Survey Professional Paper 294-B. US Geological Survey: Reston, VA.

Hack JT. 1957. *Studies in Longitudinal Stream Profiles in Virginia and Maryland*, US Geological Survey Professional Paper 294-B. US Geological Survey: Reston, VA.

Harrison LR, Keller EA. 2007. Modelling forced pool-riffle hydraulics in a boulder bed stream, southern California. *Geomorphology* **83**: 232–248.

Heritage GL, Milan DJ, Large ARG, Fuller I. 2009. Influence of survey strategy and interpolation model upon DEM quality. *Geomorphology* **112**: 334–344.

Hey RD. 1982. Discussion to BJ Bluck, Texture of gravel bars in braided streams. In Gravel-bed Rivers, Hey RD, Bathurst JC, Thorne CR (eds). John Wiley & Sons: Chichester; 354.

Hirsch PJ, Abrahams AD. 1984. The properties of bed sediments in pools and riffles. *Journal of Sedimentary Petrology* **51**: 757–760.

Hodge R, Sear DA, Leyland J. 2012. Spatial variations in surface sediment structure in riffle-pool sequences: a preliminary test of the Differential Sediment Entrainment Hypothesis (DSEH). *Earth Surface Processes and Landforms*. DOI:10.1002/esp.3290

Jackson WL, Beschta RL. 1982. A model of two-phase bedload transport in an Oregon Coast Range stream. *Earth Surface Processes and Landforms* **7**: 517–527.

Keller EA. 1971. Areal sorting of bed-load material: the hypothesis of velocity reversal. *Geological Society of America Bulletin* **82**: 753–756.

Keller EA. 1972. Areal sorting of bed-load material: the hypothesis of velocity reversal. A reply. *Geological Society of America Bulletin* **83**: 915–918.

Keller EA. 1982. Bed material sorting in pools and riffles. *Journal of the Hydraulics Division, American Society of Civil Engineers* **109**: 1243–1245.

Keller EA, Florsheim JL. 1993. Velocity-reversal hypothesis: a model approach. *Earth Surface Processes and Landforms* **18**: 733–740.

Lamarre H, MacVicar B, Roy AG. 2005. Using passive integrated transponder (PIT) tags to investigate sediment transport in gravel-bed rivers. *Journal of Sedimentary Research* **75**(4): 736–741.

Lamarre H, Roy AG. 2008. The role of morphology on the displacement of particles in a step-pool river system. *Geomorphology* **99**: 270–279.

Lane SN, Hardy RJ, Ferguson RI, Parsons DR. 2005. A framework for model verification and validation of CFD schemes in natural open channel flows. In *Computational Fluid Dynamics*: *Applications in Environmental Hydraulics*, Bates, PD, Lane SN, Ferguson RI (eds). John Wiley & Sons: Chichester; 161–192.

Leopold LB, Wolman MG, Miller JP. 1964. Fluvial Processes in Geomorphology. W.H. Freeman and Co.: San Francisco, CA.

Lisle TE. 1979. A sorting mechanism for riffle-pool sequence. *Geological Society of America Bulletin* **90**: 1142–1157.

Lisle TE, Hilton S. 1992. The volume of fine sediment in pools: an index of sediment supply in gravel-bed streams. *Water Resources Bulletin* **28**(2): 371–383.

MacVicar BJ, Roy AG. 2007a. Hydrodynamics of a forced riffle pool in a gravel bed river: 1. Mean velocity and turbulence intensity. *Water Resources Research* **43**: W12401.

MacVicar BJ, Roy AG. 2007b. Hydrodynamics of a forced riffle pool in a gravel bed river: 2. Scale and structure of coherent turbulent events. *Water Resources Research* **43**: W12402.

MacVicar BJ, Roy AG. 2010. Sediment mobility in a forced riffle-pool. *Geomorphology* **125**: 445–456.

MacWilliams ML, Wheaton JM, Pasternack GB, Street RL, Kitanidis PK. 2006. Flow convergence routing hypothesis for pool-riffle maintenance in alluvial rivers. *Water Resources Research* **42**: W10427.

Milan DJ. 2000. Sand and Gravel Transport through a Riffle-pool Sequence, Unpublished PhD Thesis, Department of Geography, University of Newcastle upon Tyne; 341 pp.

Milan DJ, Heritage GL, Large ARG. 2002. Tracer pebble entrainment and deposition loci: influence of flow character and implications for riffle-pool maintenance. In *Sediment Flux to Basins*: *Causes*, *Controls and Consequences*, Jones SJ, Frostick LE (eds), Geological Society of London Special Publications 191. The Geological Society: London; 133–148.

Milan DJ, Heritage GL, Large ARG, Charlton ME. 2001. Stage-dependent variability in shear stress distribution through a riffle-pool sequences. *Catena* **44**: 85–109.

Milan DJ, Heritage GL, Large ARG, Fuller ID. 2011. Filtering spatial error from DEMs; implications for morphological change estimation. *Geomorphology* **125**: 160–171.

Milne JA. 1982. Bed material size and the riffle/pool sequence. *Sedimentology* **29**: 267–278.

Montgomery DR, Buffington JM, Smith RD, Schmidt KM, Pess G. 1995. Pool spacing in forest channels. *Water Resources Research* **31**: 1097–1105.

Olsen NRB. 2004. A three-dimensional numerical model for simulation of sediment movements in water intakes with multi-block option. SSIIM Users Manual Version 1.1 and 2.0.

Olsen NRB. 2007. *A Three-dimensional Numerical Model of Sediment Movements in Water Intakes with Multiblock Option – User's Manual Version 1.1*. Department of Hydraulic and Environmental Engineering, The Norwegian University of Science and Technology: Trondheim.

Olsen NRB, Kjellesvig HM. 1998. Three dimensional numerical flow modelling for estimation of local scour depth. *Journal of Hydraulic Research* **33**: 571–581.

Pasternack GB, Bounrisavong MK, Parikh KK. 2008. Backwater control on riffle-pool hydraulics, fish habitat quality, and sediment transport regime in gravel-bed rivers. *Journal of Hydrology* **357**: 125–139.

Patanker SV. 1980. Numerical Heat Transfer and Fluid Flow. McGraw-Hill: New York.

Petit F. 1987. The relationship between shear stress and the shaping of a pebble-loaded river La Rulles-Ardenne. *Catena* **14**: 453–468.

Richards KS. 1976a. The morphology of riffle-pool sequences. *Earth Surface Processes and Landforms* **1**: 71–88.

Richards KS. 1976b. Channel width and the riffle-pool sequence. *Geological Society of America Bulletin* **87**: 883–890.

Richards KS. 1978. Simulation of flow geometry in a riffle-pool stream. *Earth Surface Processes and Landforms* **3**: 345–354.

Robert A. 1997. Characteristics of velocity profiles along riffle-pool sequences and estimates of bed shear stress. *Geomorphology* **19**: 89–98.

Sear DA. 1996. Sediment transport processes in pool-riffle sequences. *Earth Surface Processes and Landforms* **21**: 241–262.

Sear DA, Damon W, Booker DJ, Anderson DG. 2000. A load cell based continuous recording bedload trap. *Earth Surface Processes and Landforms* **25**: 659–672.

Sear DA, Newson MD. 2004. The hydraulic impact and performance of a lowland rehabilitation scheme based on pool-riffle installation: the River Waveney, Scole, Suffolk, UK. *River Research and Applications* **20**(7): 847–863.

Teisseyre AK. 1984. The River Bobr in the Blazkowa study reach (central Sudetes): a case study in fluvial processes and fluvial sedimentology. *Geological Sudetica* **19**: 7–71.

Teleki PG. 1972. Areal sorting of bed-load material: the hypothesis of velocity reversal: discussion. *Geological Society of America Bulletin* **83**: 911–914.

Thompson DM. 2007. The characteristics of turbulence in a shear zone downstream of a channel constriction in a coarse-grained forced pool. *Geomorphology* **83**: 199–214.

Thompson DM. 2011. The velocity reversal hypothesis revisited. *Progress in Physical Geography* **35**: 123–132.

Thompson DM, Wohl EE, Jarrett RD. 1996. A revised velocity-reversal and sediment-sorting model for a high gradient, pool-riffle stream. *Physical Geography* **17**: 142–156.

Thompson DM, Wohl EE, Jarrett RD. 1999. Velocity reversals and sediment sorting in pools and riffles controlled by channel constrictions. *Geomorphology* **27**: 229–241.

Warton DI, Wright IJ, Falster DS, Westoby M . 2006. Bivariate line-fitting methods for allometry. *Biological Reviews* **81**(2): 259–291.

Wheaton JM, Pasternack GB, Merz JE. 2004a. Spawning habitat rehabilitation – II. Using hypothesis testing and development in design, Mokelumne River, California, U.S.A. *International Journal of River Basin Management* **2**(1): 21–37.

Wheaton JM, Pasternack GB, Merz JE. 2004b. Spawning habitat rehabilitation – I. Conceptual approach and methods. *International Journal of River Basin Management* **2**(1): 3–20.

Wilkinson SN, Keller RL, Rutherford ID. 2000. Predicting the behaviour of the riffle-pool sequence in natural rivers: a conceptual approach. In New trends in water and environmental engineering for safety and life, Maione U, Lehto B, Monti R (eds). Balkema, Rotterdam.

Wilkinson SN, Keller RJ, Rutherford ID. 2004. Phase-shifts in shear stress as an explanation for the maintenance of pool-riffle sequences. *Earth Surface Processes and Landforms* **29**: 737–753.

Wilkinson SN, Rutherford ID, Keller RJ. 2008. An experimental test of whether bar instability contributes to the formation, periodicity and maintenance of pool-riffle sequences. *Earth Surface Processes and Landforms* **33**: 1742–1756.

Wolman MG. 1954. A method of sampling coarse river gravels. *Transactions of the American Geophysical Union* **35**: 951–956.

Yang CT. 1971. Formation of riffles and pools. *Water Resources Research* **7**: 1567–1574.